

DESIGN OF A NOVEL PIEZOELECTRIC ENERGY  
HARVESTING DEVICE FOR LOW FREQUENCY  
ENVIRONMENTS

BRAD WHITTLE







# NOTE TO USERS

This reproduction is the best copy available.

**UMI**<sup>®</sup>



**Design of a Novel Piezoelectric Energy Harvesting  
Device for Low Frequency Environments**

by

©Brad Whittle  
St. John's, Newfoundland, Canada

B.Eng., Memorial University of Newfoundland (2004)

A thesis submitted to the  
School of Graduate Studies  
in partial fulfillment of the  
requirements for the degree of  
Master of Engineering

Faculty of Engineering and Applied Science  
Memorial University of Newfoundland

May 2006



Library and  
Archives Canada

Bibliothèque et  
Archives Canada

Published Heritage  
Branch

Direction du  
Patrimoine de l'édition

395 Wellington Street  
Ottawa ON K1A 0N4  
Canada

395, rue Wellington  
Ottawa ON K1A 0N4  
Canada

*Your file* *Votre référence*  
*ISBN: 978-0-494-30517-1*  
*Our file* *Notre référence*  
*ISBN: 978-0-494-30517-1*

#### NOTICE:

The author has granted a non-exclusive license allowing Library and Archives Canada to reproduce, publish, archive, preserve, conserve, communicate to the public by telecommunication or on the Internet, loan, distribute and sell theses worldwide, for commercial or non-commercial purposes, in microform, paper, electronic and/or any other formats.

The author retains copyright ownership and moral rights in this thesis. Neither the thesis nor substantial extracts from it may be printed or otherwise reproduced without the author's permission.

#### AVIS:

L'auteur a accordé une licence non exclusive permettant à la Bibliothèque et Archives Canada de reproduire, publier, archiver, sauvegarder, conserver, transmettre au public par télécommunication ou par l'Internet, prêter, distribuer et vendre des thèses partout dans le monde, à des fins commerciales ou autres, sur support microforme, papier, électronique et/ou autres formats.

L'auteur conserve la propriété du droit d'auteur et des droits moraux qui protègent cette thèse. Ni la thèse ni des extraits substantiels de celle-ci ne doivent être imprimés ou autrement reproduits sans son autorisation.

---

In compliance with the Canadian Privacy Act some supporting forms may have been removed from this thesis.

Conformément à la loi canadienne sur la protection de la vie privée, quelques formulaires secondaires ont été enlevés de cette thèse.

While these forms may be included in the document page count, their removal does not represent any loss of content from the thesis.

Bien que ces formulaires aient inclus dans la pagination, il n'y aura aucun contenu manquant.

  
**Canada**

# **Design of a Novel Piezoelectric Energy Harvesting Device for Low Frequency Environments**

by

Brad Whittle

St. John's, Newfoundland, Canada

## **Abstract**

The advent of low-power wireless sensor technology has opened the door for new power harvesting technologies. This thesis explores three different types of piezoelectric power harvesting designs, namely the cantilever beam, cymbal transducer, and a new design referred to as a carriage spring, and compares them rigorously through the use of computer simulation software. The carriage spring design proves to have the benefit of increased mechanical-to-electrical power conversion and easily adjustable resonance frequency. Consequently, such a design is modeled through a Design of Experiments (DOE) statistical regression analysis and is then investigated further by physical experimentation.

Thesis Supervisor: Claude Daley

Title: Chair, Ocean and Naval Architectural Engineering

Thesis Supervisor: Vlastimil Masek

Title: Associate Professor, Instrumentation Control and Automation (INCA) Lab

## Acknowledgments

Throughout this work, I had an opportunity to collaborate with a wide range of people across many different disciplines. My supervisors, Dr. Daley and Dr. Masek, were always there to offer both their technical, and most importantly, their moral support throughout the graduate research process. Claude's enthusiasm towards the commercial potential of this project was a definite confidence boost during the more difficult times.

Dr. Swamidas and Dr. Budipriyanto always made time to instruct me on how to set up and use all the mechanical and electrical equipment necessary to conduct my vibration tests. In fact, without their help, the experimentation process would have definitely been next to impossible.

Everyone in technical services went far beyond the call of duty to help me design and fabricate the various mechanical components necessary for my experiments. I would especially like to thank Dave Snook, Billy Bidgood, and Doug Bolger, who were very patient with my almost daily, sometimes hourly, shop visits.

My colleagues, Eranda Harinath, Xiang Fang, Mark O'Rielly, and Jennifer Canning all contributed in their own way. Eranda's knowledge about power engineering proved very useful for this project while Scott's ability to answer *any* question, no matter how obscure, was nothing short of incredible. Mark, on the other hand, was with me every step of the way over the past two years and had to endure every crazy, unresearched, unrealistic idea I felt I needed to talk about. Jen, the one who originally proposed that I should investigate doing a masters degree, provided nothing less than full encouragement throughout my studies.

Finally, my parents deserve to be acknowledged for going out of their way to provide as close to a distraction-free atmosphere as possible in which to study. This included everything from keeping me fed during the busy times to ensuring that the weekly car repairs were completed in time for me to get to class. Both my B. Eng and M. Eng would not have been possible without their support.

# Contents

<b>1</b>	<b>Introduction</b>	<b>1</b>
1.1	Energy Harvesting Techniques . . . . .	2
1.1.1	Solar . . . . .	3
1.1.2	Acoustic . . . . .	3
1.1.3	Temperature . . . . .	3
1.1.4	Vibration . . . . .	4
1.1.5	Nuclear . . . . .	4
1.1.6	Batteries . . . . .	5
1.1.7	Conclusions Regarding Long-Life Micro-Power Sources . . . . .	5
1.2	Vibration Energy Harvesting Theory . . . . .	6
1.2.1	Generic Mechanical-to-Electrical Power Conversion . . . . .	6
1.2.2	Electromagnetic Energy Conversion . . . . .	10
1.2.3	Electrostatic Energy Conversion . . . . .	11
1.2.4	Piezoelectric Energy Conversion . . . . .	12
1.2.5	Conclusions Regarding Vibrational Energy Harvesting Techniques	19
<b>2</b>	<b>Review of Related Work</b>	<b>20</b>
2.1	Early Piezoelectric Energy Harvesting . . . . .	20
2.2	Piezoelectric Cantilever Beam . . . . .	22
2.3	Piezoelectric Cymbal . . . . .	27

<b>3</b>	<b>Design Investigation</b>	<b>30</b>
3.1	Modeling in ANSYS . . . . .	31
3.1.1	Ansys Preprocessing . . . . .	32
3.1.2	Element Selection . . . . .	33
3.1.3	Material Selection . . . . .	34
3.1.4	Defining Material Constants . . . . .	35
3.1.5	Meshing . . . . .	36
3.1.6	Solving the Problem . . . . .	37
3.1.7	Analysing the Results . . . . .	37
3.2	Energy Harvester Design Comparison . . . . .	38
3.2.1	Piezoelectric Layering Selection . . . . .	38
3.2.2	Poling Configurations . . . . .	40
3.2.3	Mechanical-to-Electrical Power Conversion . . . . .	41
3.2.4	Resonance Frequency Design . . . . .	45
3.2.5	Conclusions Regarding Energy Harvesters . . . . .	47
3.3	Detailed Carriage Spring Resonance Investigation via DOE . . . . .	48
3.3.1	Setting up the Problem . . . . .	49
3.3.2	Sum of Squares . . . . .	50
3.3.3	ANOVA Analysis . . . . .	51
3.3.4	Results . . . . .	52
3.3.5	Optimization . . . . .	56
3.3.6	Conclusions Regarding DOE . . . . .	57
<b>4</b>	<b>Experimental Results</b>	<b>59</b>
4.1	Prototype Design . . . . .	59
4.2	Experimental Setup . . . . .	62
4.2.1	Mechanical Setup . . . . .	64
4.2.2	Electrical Setup . . . . .	66
4.3	Experimentation . . . . .	67

4.3.1	Resonance Frequency Analysis . . . . .	67
4.3.2	Electrical Analysis . . . . .	70
4.3.3	Maximum Mechanical-to-Electrical Conversion . . . . .	74
4.3.4	Efficiency Investigation . . . . .	76
<b>5</b>	<b>Conclusions and Future Work</b>	<b>81</b>
5.1	Energy Harvester Design Conclusions . . . . .	81
5.2	Future Investigation . . . . .	84
<b>A</b>	<b>Ansys Carriage Spring Code</b>	<b>86</b>
<b>B</b>	<b>DOE Diagnostic Analysis</b>	<b>95</b>
<b>C</b>	<b>Bridge-Free AC-DC Power Conversion</b>	<b>100</b>
	<b>List of References</b>	<b>104</b>

# List of Figures

1-1	Schematic of generic vibration converter [2] . . . . .	7
1-2	Schematic of an electromagnetic energy converter [9] . . . . .	11
1-3	Schematic of an electrostatic energy converter [2] . . . . .	12
1-4	Piezoelectric disk (a) after poling, (b) during compression and tension, (c) with applied voltage [11] . . . . .	13
1-5	Piezoelectric axis orientation . . . . .	15
1-6	Piezoelectric circuit representation [2] . . . . .	16
1-7	Piezoelectric cantilever beam energy harvester shown in a (a) 2-D view and (b) 3-D view . . . . .	17
1-8	Piezoelectric cymbal energy harvester shown in a (a) 2-D view and (b) 3-D view . . . . .	18
2-1	Schematic diagram showing power conditioning electronics and encoder circuitry of a self powered RFID tag [15] . . . . .	21
2-2	Adaptive controller implementation in Simulink [17] . . . . .	23
2-3	Emitted electrons collecting on a cantilever beam [6] . . . . .	25
2-4	Electrical model of piezoelectric cantilever beam [23] . . . . .	26
2-5	Comparison of the displacement values of different end cap designs [24]	27
2-6	Diagram of (a) dimensions of the cymbal transducer and (b) designed holder for a cymbal transducer [26] . . . . .	28

3-1	Piezoelectric carriage spring energy harvester shown in a (a) 2-D view and (b) 3-D view . . . . .	31
3-2	Poling directions for series and parallel extender and bender designs .	40
3-3	Bending generator (a) X-stress distribution, (b) voltage distribution, (c) zoomed X-stress distribution (d) zoomed voltage distribution . . .	42
3-4	Extending generator (a) X-stress distribution, (b) voltage distribution, (c) zoomed X-stress distribution (d) zoomed voltage distribution . . .	43
3-5	Comparison of extender vs. bender voltage distributions . . . . .	44
3-6	Resonance frequency comparison of different energy harvester designs	45
3-7	Cross-sectional view of cymbal energy harvester . . . . .	49
3-8	Mass and cap height vs. resonance frequency via (a) 2-D graph and (b) 3-D graph . . . . .	53
3-9	Mass and cap thickness vs. resonance frequency via (a) 2-D graph and (b) 3-D graph . . . . .	54
3-10	Surface length and cap height vs. resonance frequency via (a) 2-D graph and (b) 3-D graph . . . . .	55
4-1	Experimental dimensions of carriage spring prototype . . . . .	60
4-2	Carriage spring end caps assembly showing (a) actual assembly and (b) CAD representation . . . . .	61
4-3	Detailed diagram of mounting bracket, shaker, and sensors . . . . .	62
4-4	Experimental setup flowchart . . . . .	63
4-5	Carriage spring mounting bracket showing (a) actual assembly and (b) CAD representations . . . . .	64
4-6	Steel test bed assembly showing (a) actual assembly and (b) CAD representation . . . . .	65
4-7	Various electrical equipment utilized during experimentation . . . . .	67
4-8	Energy harvester (a) frequency response and (b) correlation . . . . .	68
4-9	Energy harvester resonances vs. mass . . . . .	69

4-10	Energy harvester DC (a) $V_{oc}$ circuit, (b) $V_{bridge}$ circuit, (c) $V_{oc}$ output voltage, and (d) $V_{bridge}$ output voltage . . . . .	71
4-11	Energy harvester DC (a) $V_{cap}$ circuit, (b) $V_{opt}$ circuit, (c) $V_{cap}$ output voltage, and (d) $V_{opt}$ output voltage . . . . .	72
4-12	Energy harvester DC (a) voltage output and (b) power output . . . . .	73
4-13	Energy harvester AC (a) $V_{oc}$ circuit, (b) $V_{opt}$ circuit, (c) $V_{oc}$ output voltage, and (d) $V_{opt}$ output voltage . . . . .	75
4-14	Theoretical power vs. base acceleration . . . . .	77
4-15	Maximum power output vs. base acceleration for an (a) AC circuit and (b) DC circuit . . . . .	78
4-16	Energy harvester efficiency vs. base acceleration for an (a) AC circuit and (b) DC circuit . . . . .	79
4-17	Optimal resistance vs. base acceleration for an (a) AC circuit and (b) DC circuit . . . . .	80
B.1	Normal probability plot . . . . .	95
B.2	Residuals vs. predicted . . . . .	96
B.3	Residuals vs. run . . . . .	97
B.4	Predicted vs. actual . . . . .	98
B.5	Box-Cox graph . . . . .	99
C.1	Proposed mechanical-electrical design showing (a) thin conduction filaments on a cantilever beam and (b) electrical wiring . . . . .	101
C.2	Proposed mechanical-electrical design showing (a) upward position and (b) downward position . . . . .	102

# List of Tables

1.1	Comparison of energy scavenging and energy storage methods [2] . . .	2
3.1	Comparison of different piezoelectric materials [29], [30], [31] . . . . .	35
3.2	Material constants used for Ansys modeling . . . . .	36
3.3	Levels, factors, and ranges for $2^4$ design . . . . .	50
3.4	Sequential model sum of squares . . . . .	51
3.5	ANOVA table . . . . .	52
3.6	Optimized designs for lowest resonance frequency . . . . .	56
3.7	Optimized designs for 100Hz resonance frequency with minimal mass	57
4.1	Experimental end cap dimensions . . . . .	60
4.2	Experimental maximum power data . . . . .	76
4.3	Data pertaining to prototypes loaded with three different masses . . .	76
4.4	Efficiencies of three different prototypes . . . . .	78

# Chapter 1

## Introduction

Structural health monitoring has grown immensely in popularity over the past few years. Such monitoring enables both the industrial and scientific community to obtain large amounts of information which help explain the underlying phenomena present in modern civil structures. Unfortunately, today's monitoring systems consist of only a few high-powered, high-priced sensors that are hardwired to a central system. This leads to structural health monitoring systems that are extremely expensive, difficult to install, and even more difficult to maintain.

The method proposed to eliminate these issues lies in the formation of low-cost wireless sensor networks. However, the main problem with these networks is that of power. Even very expensive batteries, regardless of use, will degrade substantially within 2–5 years after installation [1]. As a result, changing thousands of batteries in hard-to-access places is not always feasible. Fortunately, a new engineering standard, IEEE 802.15.4 (Zigbee), promises to alleviate the problem by incorporating new technologies that drastically reduce power usage for wireless sensor applications. The advent of this technology has now made *battery-free* wireless communication and sensing feasible using advanced energy harvesting techniques.

The main advantage of a Zigbee-based energy harvesting system is that such a sensor network will continue to produce its own energy from the environment for the

entire lifetime of the structure, thus eliminating the need to replace batteries. These plug-and-play wireless systems will enable thousands of distributed sensors to replace existing localized sensor networks. These networks will pave the way for real time finite element modeling of structures which has the potential to produce massive cost savings for companies who agree to adopt the technology. The notion of real time accurate modeling can provide invaluable information to maintenance personnel, engineers, accident investigators, structural inspectors, and insurance companies who rely heavily on large amounts of detailed data to carry out their respective responsibilities.

## 1.1 Energy Harvesting Techniques

There are many ways to convert one form of naturally occurring energy into electrical energy. Table 1.1 gives a comparison of the energy densities associated with various energy harvesting techniques.

	<b>Power Density (<math>\mu W/cm^3</math>) 1 year lifetime</b>	<b>Power Density (<math>\mu W/cm^3</math>) 10 year lifetime</b>
Solar (Outdoors) <sup>1</sup>	15,000 - direct sun 150 - cloudy day	15,000 - direct sun 150 - cloudy day
Solar (Indoors) <sup>1</sup>	6 - office desk	6 - office desk
Acoustic Noise	0.003 @ 75 Db 0.96 @ 100 Db	0.003 @ 75 Db 0.96 @ 100 Db
Daily Temp. Variation	10	10
Temperature Gradient	15 @ 10 deg C	15 @ 10 deg C
Vibrations	200	200
Batteries (non-recharge. Lithium)	45	3.5
Batteries (rechargeable Lithium)	7	0
Hydrocarbon fuel (micro heat engine)	333	33
Fuel Cells (methanol)	280	28
Nuclear Isotopes (uranium)	$6 \times 10^6$	$6 \times 10^5$

Table 1.1: Comparison of energy scavenging and energy storage methods [2]

---

<sup>1</sup>Solar power density is in units of  $\mu W/cm^2$

### 1.1.1 Solar

During peak hours, the power density of solar radiation on the Earth's surface is approximately  $100mW/cm^2$  [2]. This seems very promising as silicon solar cells are a relatively mature technology with efficiencies ranging from 12%–25% [2]. However, this option is not practical in most industrial environments. In most industrial settings, sensors of interest are most likely placed on steel girders that are usually encased by walls or other coverings, thus eliminating most useful light. Also, solar cells need to be kept relatively clean in order to have direct access to the sun. This rules out most outdoor applications as rain, dirt, debris, and snow will cause substantial power losses on the solar cell's surface.

### 1.1.2 Acoustic

There is far too little air-borne acoustic noise in most civil structures to generate any significant amount of power. This section was included in the discussion for the sake of completeness in covering most common forms of energy harvesting and is not considered a viable energy producing source at this time.

### 1.1.3 Temperature

Temperature gradients are actually quite common on many structures and can be a viable source of energy. Applied Digital [3], a New York-based company, is currently making great strides in developing thermopile technology for use in wireless sensor and Zigbee applications. A recent press release claims that a  $9.6mm$  diameter thermopile can produce  $100\mu W$  of DC power with only a 5 degree Celsius temperature difference [3]. This technology may find its way into certain civil structure monitoring applications; however, it is more likely to be used in circumstances where there is an abundant temperature difference. These applications may include large industrial motors, muffler manifolds, building heating and cooling ducts, as well as furnaces

and heating elements. In fact, the United States Department of Energy is currently funding projects in which thermoelectric energy harvesters obtain power from the temperature gradients between sea water cooled ship hulls and the surrounding air. Although this may be a very viable technology, it is currently quite expensive and has energy densities far less than other alternatives.

#### **1.1.4 Vibration**

Vibrational energy appears to have great potential for industrial applications where vibrating equipment, machinery, and structures are commonplace. For marine applications, diesel engines in marine vessels cause the entire ship hull to vibrate and open the doors for potential vibrational energy harvesting techniques. Also, aircraft wings, automobiles, and rail tracks provide high vibration levels that have great potential for converting wasted vibration energy into electrical power. Although much research has gone into vibrational energy harvesting using magnetic resonators, piezoelectric vibrational energy harvesters have proven to be much more efficient over the past few years. The research in this area has evolved from passive human power (piezoelectrics in shoes) for army applications to multi-resonant high efficiency cymbal energy harvesters for high vibration applications.

#### **1.1.5 Nuclear**

One of the most promising technologies to tackle the wireless sensor powering problem is that of micro nuclear batteries, also known as betavoltaics. Although betavoltaic batteries have been around since the 1950's, they were very inefficient until recent years. Sun, et al (2005), released a paper in which they tested chemically etching deep pores in the p-n junction of the porous silicon used to turn the beta rays of the radioisotope into electricity. The pores increased efficiency by over 200 times in its crude form [4]. In fact, the authors of the paper have since formed a Houston-based company, known as Betabatt Inc [5]. The company claims to be developing

batteries for industrial applications that will produce up to  $125\mu W/cm^3$  of power and last between 12 and 100 years, depending on the application. Other researchers have also experimented with utilizing piezoelectric biomorph beams with nuclear isotopes [6]. This technique is discussed further in the literature review section. Although nuclear batteries may be looked upon as a dangerous technology, they are actually quite safe as the beta rays emitted by most isotopes being used in the devices will not even penetrate a piece of paper. This technology seems very promising and much work should be done in this field if a truly economic solution to the wireless sensor powering challenge is to be developed.

### **1.1.6 Batteries**

Batteries, as well as fuel cells, share the same problem of having to be recharged. In addition to this problem, a battery undergoes oxidization over time and after a few years will become unchargeable and will have to be replaced. This is a very impractical and uneconomical practice, especially in a harsh industrial environment. However, in some applications, one may want to use an energy harvester to trickle-charge a battery that may be used very infrequently but require a lot of power. Some organizations, including the Defense Advanced Research Projects Agency (DARPA), are researching solid state Lithium thin-film batteries that have extra long lifetimes and can be charged tens of thousands of times with minimal leakage [7]. Other new technologies that have emerged are small super-capacitors that have a very large capacitance and can also be recharged almost indefinitely.

### **1.1.7 Conclusions Regarding Long-Life Micro-Power Sources**

The choice of energy harvesting depends on the application. Solar, acoustic, and traditional lithium batteries seem very impractical for most industrial civil structure monitoring applications. Thermopiles have undergone many advancements in recent years and may prove to be quite adequate for some applications, especially high-

temperature gradient industrial applications. However, it is the author's opinion that either a combination of vibrational energy harvesters with thin-film batteries or nuclear batteries will be the future for powering wireless sensor networks in a civil structure monitoring environment. Vibrational energy harvesters may find their way in many applications in which a large vibration level is present. However, for more static applications, such as building monitoring, nuclear batteries may be more reliable and effective at powering such sensor networks.

## **1.2 Vibration Energy Harvesting Theory**

There are three main methods that are typically used to harvest energy from vibration. They are electromagnetic (inductive), electrostatic (capacitive), and piezoelectric. These methods are typically used to create actuators or sensors, but can also be used for energy conversion. Before any specific discussion on these techniques can take place, the generic mechanical-to-electrical power conversion model must first be discussed.

### **1.2.1 Generic Mechanical-to-Electrical Power Conversion**

An excellent discussion on mechanical-to-electrical power generation is given in a 1995 journal by Williams and Yates [8] and is thoroughly investigated by Roundy [2]. Figure 1-1 gives a schematic of a generic vibration energy harvester, and the equation of motion is given by Equation 1.1.

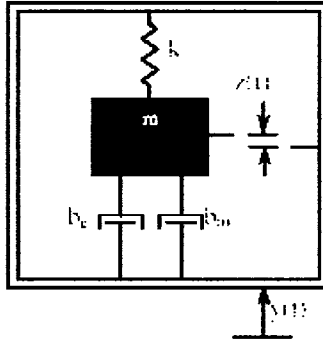


Figure 1-1: Schematic of generic vibration converter [2]

$$m\ddot{z} + (b_e + b_m)\dot{z} + kz = -m\ddot{y} \quad (1.1)$$

where

$m = \text{mass [kg]}$

$z = \text{mass deflection [m]}$

$b_e = \text{electrical damping [Ns/m]}$

$b_m = \text{mechanical damping [Ns/m]}$

$k = \text{spring constant [N/m]}$

$y = \text{input displacement [m]}$

The model states that any energy conversion that takes place is due to net movement of the mass relative to the generator housing. The power converted to the electrical system is equal to mechanical power removed from the system by the electrically induced damping. In other words, the conversion of mechanical-to-electrical energy looks like a linear damper from the mass-spring system [2]. Although this linear model is not exactly correct for some types of converters, it does aid in drawing meaningful conclusions regarding generators as a whole. If broadband frequencies are ignored and it is assumed that the generator is excited by only a single frequency in

the form  $y(t) = Y_0 \cos(\omega t)$ , then the output power is given as

$$|P| = \frac{m\zeta_e \omega_n \omega^2 \left(\frac{\omega}{\omega_n}\right)^3 Y_0^2}{\left(2\zeta_T \frac{\omega}{\omega_n}\right) + \left(1 - \left(\frac{\omega}{\omega_n}\right)^2\right)^2} \quad (1.2)$$

where

$|P|$  = magnitude of power [W]

$\zeta_e$  = electrical damping ratio [-]

$\omega_n$  = natural frequency of the system [rad/s]

$\omega$  = frequency of the base driving vibrations [rad/s]

$Y_0$  = displacement of the base driving vibrations [m]

$\zeta_T$  = total damping ratio ( $\zeta_T = \zeta_e + \zeta_m$ ) [-]

If the resonant frequency of the generator is equal to the frequency of the input driving vibrations, then Equation 1.2 can be simplified to form

$$|P| = \frac{m\zeta_e \omega^3 Y_0^2}{4\zeta_T^2} \quad (1.3)$$

$$|P| = \frac{m\zeta_e A_0^2}{4\omega\zeta_T^2} \quad (1.4)$$

where

$A_0$  = magnitude of input acceleration [ $m/s^2$ ]

Equations 1.3 and 1.4 can also be used to determine the maximum potential power that can be extracted from a vibration source. Normally, a harvester that could produce power near 50% of this maximum value would be considered excellent.

Power optimization of a particular generator for a specific input vibration is feasible if certain design criteria are kept in mind. Roundy [2] provides the following

functional relationships necessary for optimal converter design.

1. The system should be designed to resonate at the target driving frequency.
2. Power output is proportional to the square of the driving vibration acceleration.
3. Power output is proportional to the mass attached to the system assuming mechanical constraints are not violated. This implies that scaling down a converter can be quite a daunting task.
4. Assuming equal acceleration, the power output is inversely proportional to the frequency. Therefore, designing for lower frequencies in a given frequency spectrum is preferred assuming the same or greater acceleration.
5. The energy removed by the electrical load looks like damping to the system. The load can be designed such that the level of effective electrically induced damping maximizes power transfer to the load. This condition occurs when  $\zeta_e = \zeta_m$ . It should be noted that there is a large penalty when  $\zeta_m > \zeta_e$ ; however there is only small penalty when  $\zeta_m < \zeta_e$ .
6. A system with a low total damping ratio,  $\zeta_T$  has the potential for a higher output power; however, a system with a high  $\zeta_T$  has a larger bandwidth. In other words, if the exact frequency of the driving force is constant, then a low damping ratio is optimal. However, if the input frequency changes slightly, a highly damped system will produce less power loss as the system deviates from resonance.

### 1.2.2 Electromagnetic Energy Conversion

Faraday's Law states that any change in the magnetic environment of a coil of wire placed in a magnetic field will cause an emf (voltage) to be induced in the coil. Faraday's Law, a direct result of Maxwell's equations, is given in Equation 1.5 as.

$$emf = -N \frac{d\Phi_B}{dt} \quad (1.5)$$

where

$emf$  = electromagnetic force [V]

$N$  = number of turns in the inductor [-]

$\Phi_B$  = magnetic flux [Wb]

Electromagnetic energy harvesters take advantage of this law by placing a wound coil (inductor) on the bottom of a small spring-anchored mass. The mass and coil are then placed directly over a small permanent magnet, separated by an air gap. When motion causes the mass to vibrate, the changing gap distance causes the magnetic field experienced by the coil to be altered. The resultant open circuit voltage is given as

$$V_{oc} = NB l \frac{dy}{dt} \quad (1.6)$$

where

$V_{oc}$  = open circuit voltage [V]

$B$  = strength of the magnetic field [T]

$l$  = length of a single coil ( $2\pi r$ ) [m]

$y$  = distance the coil moves through the field [m]

Electromagnetic converters do not require any boot circuitry and are quite simple to construct. However, the voltage levels produced by such devices are normally on

the order of  $mV$ , which can make AC-DC rectification very difficult due to losses in the circuit. Figure 1-2 shows an example of an electromagnetic converter that was developed by Amirtharajah and Chandrakasan [9].

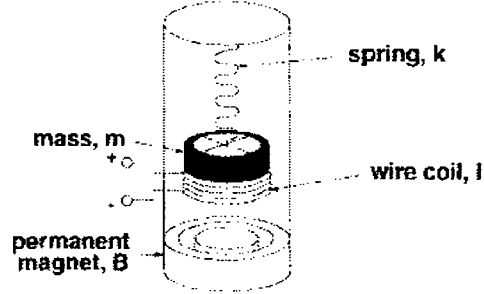


Figure 1-2: Schematic of an electromagnetic energy converter [9]

### 1.2.3 Electrostatic Energy Conversion

A capacitor, a device which is able to store charge, consists of two parallel plate conductors separated by a dielectric. The basic equation for capacitance is

$$C = \frac{\epsilon_r \epsilon_0 A}{d} \quad (1.7)$$

where

$C$  = capacitance [ $F$ ]

$\epsilon_0 = 8.854 \times 10^{-12}$  [ $F/m$ ]

$\epsilon_r$  = relative dielectric constant [-]

$A$  = area of the electrode [ $m^2$ ]

$d$  = plate separation distance [ $m$ ]

When one parallel plate is held stationary and the other is free to vibrate, a change in the plate separation causes the capacitance to change. If the charge of the capacitor is held constant and the separation distance is changed, a voltage difference

can be observed and is given by

$$V_{oc} = \frac{Q}{C} \quad (1.8)$$

where

$V_{oc}$  = voltage across the capacitor [V]

$Q$  = charge across the capacitor [F]

One distinct disadvantage of an electrostatic generator is that an external power source is needed. This is because the capacitor must first be charged up to an initial voltage in order to start the mechanical-to-electrical conversion process [2]. Figure 1-3 shows an example of an electromagnetic converter that was developed by Roundy using MEMS microfabrication techniques [2].

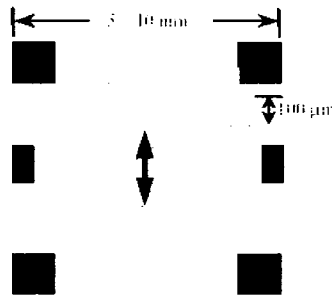


Figure 1-3: Schematic of an electrostatic energy converter [2]

#### 1.2.4 Piezoelectric Energy Conversion

The piezoelectric effect states that an AC current can be extracted from a piezoelectric material when a dynamic strain (vibration) is applied to the material. The most common types of piezoelectric materials are Lead Zirconate-Titanates (PZTs) which are solid structures composed of lead zirconate and lead titanate. These materials are created by mixing the compounds together at 800–1000 degrees Celsius. This creates

a powder which is then mixed with a binding agent and sintered into shape. Once cooled, the piezoelectric material must be poled in the appropriate direction in order for it to take on piezoelectric properties. [10]

Poling is the act of heating the material over the Curie Temperature and applying a large electric field which causes the crystals inside the material to align themselves in only one specified direction. Heating the material above the Curie temperature allows the molecules to move more freely and thus makes the poling of the material much easier. Once the material cools and the electric field is removed, the crystals remain aligned in one direction and the geometry of the unit cell remains asymmetrical.

Now, when the material is forced into compression, a voltage with the same polarity as the poling voltage will appear across the electrodes. If a tensile force is applied to the material, an opposite voltage will be produced across the electrodes. This is known as the direct piezoelectric effect [10]. If a voltage is applied to the electrodes in the same direction as the poling direction of the piezoelectric material, the material will compress. If a voltage opposite to that of the poling direction is applied to the electrodes, the material will be forced into tension. This is called the converse piezoelectric effect.

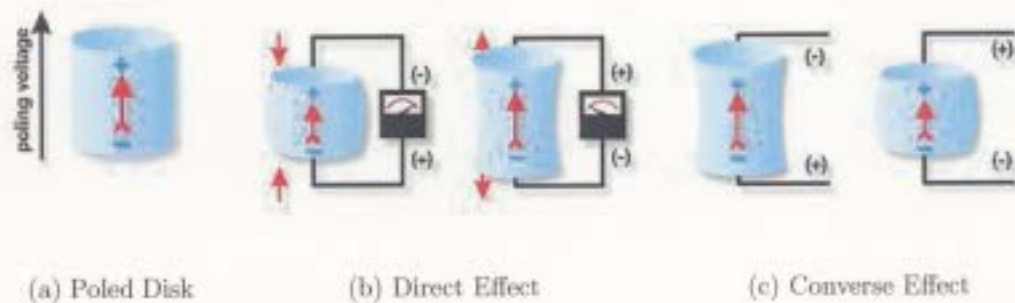


Figure 1-4: Piezoelectric disk (a) after poling, (b) during compression and tension, (c) with applied voltage [11]

The constitutive equations for a linear piezoelectric material in reduced-matrix form as presented in Tzou [12] are

$$\{S\} = [s^E] \{T\} + [d]^t \{E\} \quad (1.9)$$

$$\{D\} = [d] \{T\} + [\epsilon^T] \{E\} \quad (1.10)$$

where

$\{S\}$  = strain vector  $[m/m]$

$\{T\}$  = stress vector  $[N/m^2]$

$\{E\}$  = electric field vector  $[N/m^2]$

$\{D\}$  = electrical displacement vector  $[C/m^2]$

$[s^E]$  = elastic compliance matrix at constant electric field  $[m^2/N]$

$[d]$  = matrix of piezoelectric strain coefficients  $[m/V]$

$[\epsilon^T]$  = dielectric constant matrix at constant stress  $[F/m]$

Equation 1.9 represents the converse piezoelectric effect. In fact, if the piezoelectric coupling term,  $dE$ , is omitted, Equation 1.9 is simply Hooke's Law. Equation 1.10 represents the direct piezoelectric effect. Similarly, without the coupling term,  $dT$ , Equation 1.10 becomes Gauss' Law for electricity. The piezoelectric coupling provides a means by which energy conversion can take place in the piezoelectric material. The electric field across the material affects its mechanical behavior, while the stress in the material affects its dielectric properties [2]. The effects of these two phenomena are extremely dependent on their orientation to the poled axis. As a result, standard axis numbering must be established before continuing further with any piezoelectric theory.

Most piezoelectric coefficients of any kind are usually labeled with a double subscript, such as  $d_{ij}$ . The first subscript,  $i$ , is the electrical (poled) direction and the second subscript,  $j$ , is the mechanical direction. Figure 1-5 shows the three reference axis labeled  $X$ ,  $Y$ , and  $Z$ . The  $X$  and  $Y$  axis are usually referenced by the numbers

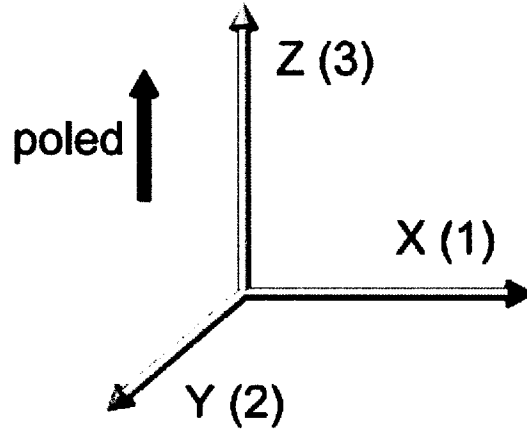


Figure 1-5: Piezoelectric axis orientation

1 and 2 respectively, while the  $Z$  axis, the pooled axis in Figure 1-5, is referenced by the number 3. There are also four other less-commonly used reference numbers. The numbers 4, 5, and 6 represent shear around the  $X$ ,  $Y$ , and  $Z$  axis respectively, while the letter  $P$  represents radial vibration. With this nomenclature, it is now possible to discuss piezoelectric *modes*. A piezoelectric mode refers to the direction of the electrical and mechanical effects. The most widely used mode for piezoelectric energy harvesters is mode-31. This mode implies that the piezoelectric material is poled along the 3-axis with the electrodes placed on the surface of the material perpendicular to the 3-axis. The piezoelectric material experiences a one-dimensional stress along the 1-axis only. Although stresses along the 3-axis and along the 5-axis are much more efficient, a thin mode-31 material is much more compliant and requires a much smaller input force to cause the material to strain. This approach is also very useful in lowering the resonance frequency of the energy harvester.

$$S_1 = s_{11}^E T_1 + d_{31} E_3 \quad (1.11)$$

$$D_3 = d_{31} T_1 + \epsilon_{33}^T E_3 \quad (1.12)$$

If only mode-31 is considered, the multi-modal matrices in Equation 1.9 and Equation 1.10 can be reduced to Equation 1.11 and Equation 1.12. These new equations are now scalar quantities and are much easier to work with. Although these assumptions may produce small errors as not all mechanical stresses are being considered, these errors are deemed insignificant.

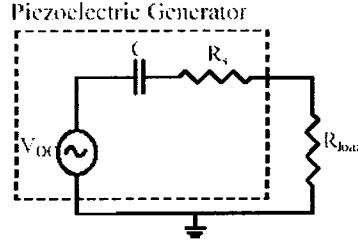


Figure 1-6: Piezoelectric circuit representation [2]

If the piezoelectric element in Figure 1-6 is subject to an open circuit condition, the electrical displacement in the poling direction,  $D_3$ , becomes zero. Equation 1.12 can now be reordered to solve for the open circuit voltage by substituting  $E_3 = V_{oc}/t_3$  and  $g_{31} = d_{31}/\epsilon_{33}$ . The resulting open circuit voltage equation becomes

$$V_{oc} = \frac{d_{31}}{\epsilon_{33}} t_3 T_1 = g_{31} t_3 T_1 \quad (1.13)$$

where

$V_{oc}$  = open circuit voltage [V]

$t_3$  = piezoelectric material thickness in the poling direction [m]

$g_{31}$  = piezoelectric voltage coefficient [Vm/N]

If the piezoelectric element undergoes a sinusoidal stress, an AC voltage appears across its terminals. If the AC voltage is then connected to a resistive load, the maximum average power in the piezoelectric material becomes

$$P_{max} = \frac{V_{load}^2}{2R_{load}} \quad (1.14)$$

where

$P_{max}$  = maximum power transferred to the load [W]

$V_{load}$  = load voltage [V]

$R_{load}$  = load resistance [ $\Omega$ ]

This maximum power transfer occurs when  $V_{load} = \frac{1}{2}V_{oc}$  and is a direct result of load resistance equaling the internal resistance of the piezoelectric element. This phenomena is normally referred to as impedance matching and is very important in circuit design. In fact, Equation 1.14 also is applicable to both the inductive and capacitive energy harvesting techniques discussed in the previous sections.

Although attaching an AC power harvesting generator directly to a resistor is an unlikely scenario, it does give a reference for comparing the power output of different harvester sizes, shapes and materials. A much more likely scenario is that the power harvester would be connected to some form of AC-DC conversion circuitry and then to a capacitor or to a charging battery. This additional circuitry will be discussed further in future chapters.

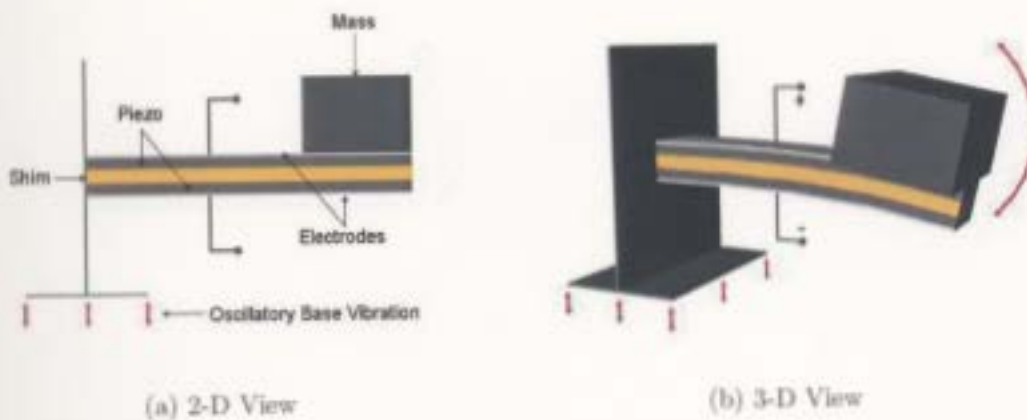


Figure 1-7: Piezoelectric cantilever beam energy harvester shown in a (a) 2-D view and (b) 3-D view

There are two typical types of mode-31 piezoelectric energy harvesters. The first consists of  $n$  layers of rectangular piezoelectric material sandwiched around a thin metallic shim. If only one end is fixed and the other is free to float with an attached mass, the device is known as a *Cantilever Beam* energy harvester. When the base of the cantilever is excited with an oscillatory forcing function, the mass also begins to oscillate. If the mass is in its downward position, as shown in Figure 1-7(b), the bottom side of the shim experiences a compressive stress while the top side is forced into tension. If wired appropriately, piezoelectric layers placed on top and bottom of this shim will generate a voltage as per equation 1.13. Layer selection and wiring considerations will be discussed in detail in Sections 3.2.1 and 3.2.2.

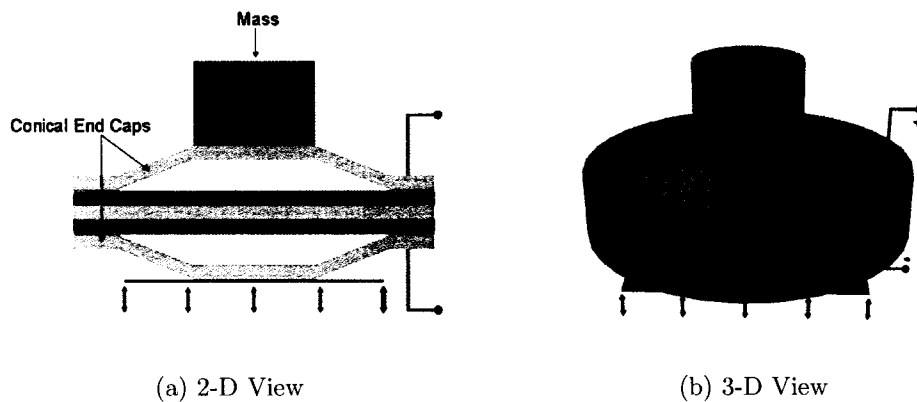


Figure 1-8: Piezoelectric cymbal energy harvester shown in a (a) 2-D view and (b) 3-D view

The second type of energy harvester is known as a *Cymbal* energy harvester. A cymbal energy harvester consists of a thin cylindrical piezoelectric material sandwiched between two conical end caps. The base of the bottom end cap is fixed to the vibrating structure while the top face of the top end cap holds a small mass. When the mass oscillates relative to the base, the end caps transfer the vertical motion into horizontal stress across the piezoelectric disk. As with the cantilever beam, this stress produces a voltage via Equation 1.13. Figure 1-8 shows a cymbal energy harvester.

### 1.2.5 Conclusions Regarding Vibrational Energy Harvesting Techniques

Piezoelectric generators can practically be produced with energy densities of  $17.7mJ/cm^3$  while electrostatic and electromagnetic generators have densities closer to  $4mJ/cm^3$  [2]. In addition, piezoelectric generators do not require a separate voltage source to begin the conversion process and can be constructed to produce any desired voltage by selecting the appropriate number of piezoelectric layers. However, one disadvantage is that microfabrication of such devices is quite difficult given today's CMOS processes [2]. This implies that mass-integration into PCBs may be a significant challenge. Conversely, electrostatic generators are very easily integrated into electronic microsystems; however, they need a separate energy source to boot the circuit and charge the system before power conversion can begin. This is a major disadvantage of electrostatic generators. Electromagnetic generators are both hard to integrate into electronic systems and produce very low voltages that make AC-DC rectification very difficult if not impossible.

It would appear that a piezoelectric energy harvesting structure seems quite promising as it has a large energy density and does not require any boot circuitry. Consequently, it was decided that a piezoelectric generator be chosen as the main focus for the research discussed in this thesis.

# Chapter 2

## Review of Related Work

### 2.1 Early Piezoelectric Energy Harvesting

Umeda [13], et al (1996), attempted to construct a device that could be used to charge portable electronics. The device consisted of a  $27mm$  diameter bronze disk that is connected to a piezoelectric patch. When a small steel ball is dropped from a distance of  $5mm$  from the disk and allowed to bounce, a bending vibration is produced in the disk. This vibration is then passed on to the piezoelectric patch and a voltage is produced. The researchers were able to generate a piezoelectric energy harvester with a maximum efficiency approaching 35%.

In a subsequent paper, Umeda [14], et al (1997), expanded on their previous research by dropping a ball from  $20mm$ . The researchers calculated that the ball had 67.5% of its kinetic energy after the bounce. In order to harness this unused energy, the authors determined that if the ball would stay in contact with the plate, a generator efficiency of over 52% could be achieved. In addition to these results, the researchers pointed out that the total output power of such a device is highly dependant on the load resistance. In fact, there exists an optimal load resistance which gives maximum efficiency. The researchers also point out that the efficiency of the device increases with an increase in mechanical quality factor,  $Q$ , and electromechanical

coupling coefficient,  $k$ .

Kymissis [15], et al (1998), investigate three different methods to harvest wasted energy from a person's step. The first method attempted to *parasitically* harvest energy due to the bending motion of the sole in a person's shoe. The second method attempted to harvest energy from a person's heel strike. To accomplish this, a small piece of piezoelectric material was connected to a curved section of thin steel. When the person's foot in the shoe presses the steel flat, the stress across the piezoelectric material produces a voltage. The third method involved an electromagnetic generator. When the heel comes in contact with the ground, a small lever cranks a rotary generator. Although this device generated almost two orders of magnitude more power than the piezoelectric generators, it did prove to be very cumbersome. The piezoelectric generators, however, were easily integrated into a running sneaker and were barely noticeable. The paper concludes by discussing the potential for incorporating RFID technology into the shoes by giving a full circuit diagram and experimental results of such a system. Figure 2-1 shows a schematic of a circuit that is used to store energy and then transmit an RFID when sufficient energy has been harvested. The work done by Kymissis was most likely the first time the properties of piezoelectric materials were explored for use in a practical energy harvesting application.

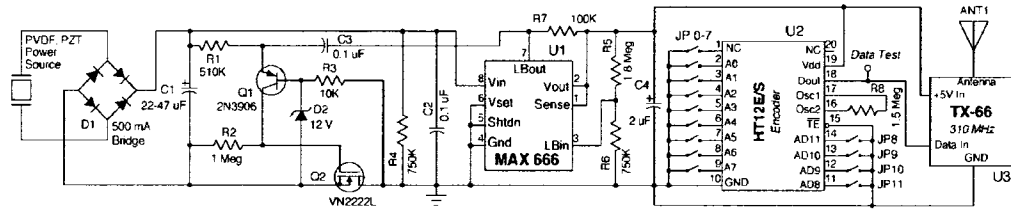


Figure 2-1: Schematic diagram showing power conditioning electronics and encoder circuitry of a self powered RFID tag [15]

## 2.2 Piezoelectric Cantilever Beam

Kasyap [16], et al (2002), investigated the feasibility of using strain energy induced in a vibrating cantilever beam as a source for energy reclamation using a flyback converter circuit. The researchers attached a  $50.8mm$  long section of PZT-5H to a  $203.2mm$  aluminum cantilever beam. The beam was then excited at  $59Hz$  and the output was passed through a flyback converter with a switching frequency of  $5.9kHz$ . A purely resistive load was then attached to the device and varied until a maximum power output was obtained. The results were then compared to a lumped element model and seemed to be in good agreement. The results also showed that the flyback converter exceeded an efficiency of 80%.

Ottman [17], et al (2002), investigated interface circuitry designed specifically for piezoelectric energy harvesting applications. An important step in piezoelectric energy harvesting is AC-DC rectification. However, due to the inherent nature of piezoelectric materials, the voltages produced are normally quite high and need to be lowered by a DC-DC converter in order to operate common electronics or trickle-charge a battery. Ottman noted that there exists an optimal switching frequency of the DC-DC converter that allows for maximum power transfer. The authors tested this hypothesis and the results appeared promising. However, Ottman realized that this optimal switching frequency relies heavily on the mechanical excitation level of the piezoelectric generator. To accommodate this phenomena, Ottman designed an algorithm in Simulink [18], shown in Figure 2-2, to actively tune the switching frequency for optimal power transfer regardless of the mechanical excitation. To test the algorithm, a small off-the-shelf cantilever was excited and the algorithm was implemented through a dSpace [19] controller board. Experimental results revealed that use of the adaptive DC-DC converter increases power transfer by over 400% as compared to when the DC-DC converter is not used.

In a subsequent paper, Ottman [20], et al (2003), built upon their existing research to implement their adaptive algorithm in stand-alone circuitry in order to trickle-

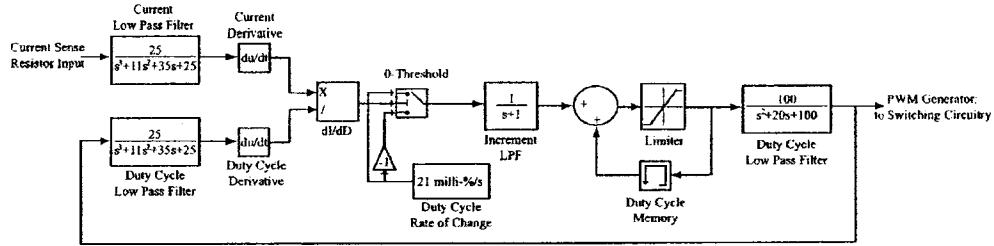


Figure 2-2: Adaptive controller implementation in Simulink [17]

charge a small battery. The researchers realized that at high mechanical excitation levels, the optimal duty cycle becomes essentially constant. Therefore, the stand-alone circuitry was designed to have a high excitation mode and a low excitation mode. When high excitation exists, the circuitry drops the voltage using a constant optimal DC-DC converter duty cycle. This circuitry requires very low power and can actually be powered by the piezoelectric material. However, when the excitation level is low, the optimal duty cycle is varying substantially and a more complex adaptive algorithm must be implemented. At these low excitation levels, losses in the DC-DC converter can easily exceed the power produced by the piezo, therefore; the DC-DC converter is bypassed and the battery is instead charged by a pulse-charging circuit. The threshold level of mechanical excitation that divides the two modes of operation will depend on the power produced by the piezoelectric element, the losses of the step-down converter, the power consumption of the control circuitry, and the optimal duty cycle stabilization at higher excitations. The authors reported that a stand-alone version of their earlier algorithm would be feasible under the right conditions. Experimental results showed an increase in harvested power of over 325%.

Eggborn [10], (2003), attached small amounts of piezoelectric material on large cantilever beams to explore three piezoelectric modeling techniques. The Pin-force, Enhanced Pin-force, and Bernoulli method were evaluated to determine the most accurate way to model the system. Through experimentation it was shown that the Bernoulli method was superior to the other two methods. By using the Bernoulli

method, Eggborn utilized Matlab [18] and Mathematica [21] to model different sizes of piezoelectric material on a large vibrating cantilever. Eggborn proved that for long beams, there existed an optimal length and thickness of piezoelectric material. Through experimentation, the researcher proved that at the far end of the beam the material began to act as a load and began to actually remove power from the system. This is because the piezoelectric material is now adversely affecting mechanical beam parameters by increasing the thickness of the beam, increasing the overall elastic modulus, and affecting resonance frequencies. This work showed the importance of optimal piezoelectric material design when dealing with long cantilever beams.

Roundy [22], et al (2002), discussed the potential for power scavenging from a variety of sources. Roundy concluded that although vibration is not the most abundant power source for energy scavenging, it does have the potential to produce large amounts of power in situations where solar cell cannot be used. The author then explores in detail the power spectral densities of various low-level vibration sources, such as microwave ovens and windows on a house. Roundy concludes that most of these commonly occurring vibration sources produce significant energy at 100–120Hz. After both quantitatively and qualitatively proving that piezoelectric generators have distinct advantages over electromagnetic and electrostatic converters, a small piezoelectric cantilever beam prototype is constructed. The prototype is capable of producing  $250\mu W/cm^3$  from a vibration source with an acceleration amplitude of  $2.5m/s^2$  at 120Hz.

Lal [6], et al (2004), used the charged particles emitted from a radioisotope to generate energy from a cantilever beam. The researchers placed a  $4mm^2$  thin film  $^{63}Ni$  radioisotope a small distance below a silicon cantilever beam. By charge conservation, the radioisotope will have a positive charge as it radiates electrons onto the cantilever. The attraction between the two oppositely charged surfaces causes the beam to approach the  $^{63}Ni$  film. Eventually, the two touch and the charge is neutralized. This causes the cantilever to spring back and begin to vibrate.

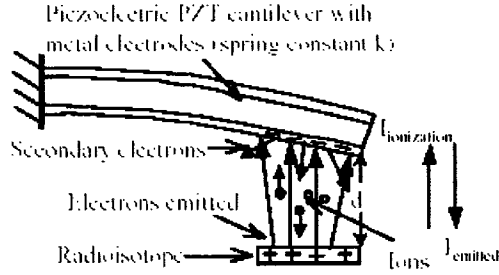


Figure 2-3: Emitted electrons collecting on a cantilever beam [6]

The addition of a piezoelectric material to the cantilever is used to convert mechanical energy into electrical energy as the device oscillates. In addition to this, the study also showed that the device simultaneously creates an RF pulse. The cantilever, built from a material with a high dielectric constant, had metal electrodes on its top and bottom. An electric field formed inside the dielectric as the bottom electrode charged. When it discharged, a charge imbalance appeared in the electrodes, making the electric field propagate along the dielectric material. The cantilever thus acted like an antenna that periodically emitted RF pulses, the interval between pulses varying according to the pressure. This led the researchers to create self-powered RF pressure sensors and microprocessors. Due to the fact that  $^{63}Ni$  has a half life of 100.2 years, these devices have the potential to last for an extremely long time without the use of external power sources.

Roundy [23], et al (2004), used a electrical circuit modeled to represent the behavior of a piezoelectric biomorph beam. This model allowed the researchers to calculate the expected electrical output based on critical beam dimensions. In Figure 2-4, the inductor,  $L_m$ , represents the mass or inertia of the generator. The equivalent resistor,  $R_b$ , represents the mechanical damping, and the capacitor,  $C_k$ , represents the mechanical stiffness of the beam. The stress generated as a result of the input vibration is shown as  $\sigma_{in}$ . The variable  $n$  represents the turns ratio of the transformer, while  $C_b$  is the capacitance of the piezoelectric bender. The entire model can be represented

by the equations

$$\sigma_{in} = L_m \ddot{S} + R_b \dot{S} + \frac{S}{C_k} + nV \quad (2.1)$$

$$i = C_b \dot{V} \quad (2.2)$$

where

$S$  = cantilever strain [ $m/m$ ]

$V$  = piezoelectric voltage [ $V$ ]

$i$  = piezoelectric current [ $A$ ]

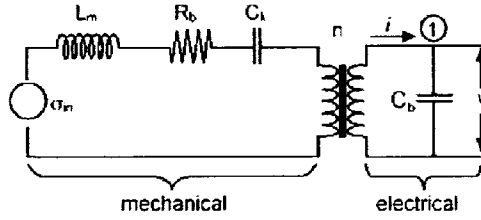


Figure 2-4: Electrical model of piezoelectric cantilever beam [23]

The authors of the article point out that most vibrations seen in industrial equipment vibrate at accelerations of approximately  $0.2-10m/s^2$  at frequencies of  $60-100Hz$ . For the purposes of this paper, two different  $1cm^3$  size piezoelectric bimorph beams are fabricated and are excited at  $2.5m/s^2$  at  $120Hz$ . The first design was wider while the second design was longer. The researchers were able to obtain over  $200\mu W$  and  $350\mu W$  respectively from the two designs. Both designs had a proof mass attached to the far end to increase strain and control the resonance frequencies. The second design was chosen to be the power source for a small pico-radio as a proof of concept for minute self-powered wireless sensor network nodes.

## 2.3 Piezoelectric Cymbal

Dogan [24], et al (1997), used finite element analysis to identify areas of high stress concentrations in the end caps of the traditional “moonie” actuator. This led researchers to develop a means by which these high stress areas could be reduced in order to transfer the stress more uniformly and efficiently by use of two new designs, the “grooved moonie” and the “cymbal” transducer. The cymbal transducer allowed for larger displacement, larger generative forces, and more cost-effective manufacturing. The experimental results of the cymbal used in this study showed a 40 times higher displacement by using a cymbal than by using a simple piezoelectric material by itself. In addition, the research showed that a cymbal could produce nearly twice as much displacement as the same sized moonie transducer. These three actuator shapes are shown in Figure [?].

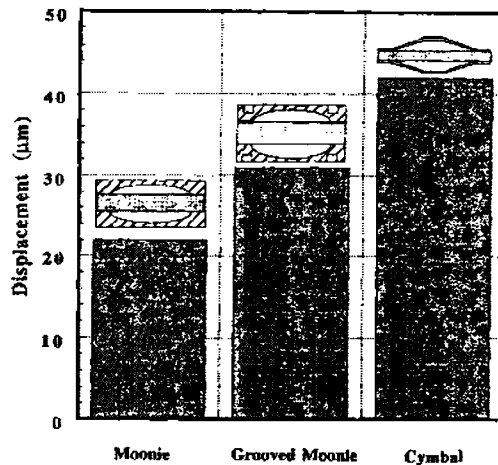


Figure 2-5: Comparison of the displacement values of different end cap designs [24]

Tressler [25], et al (1998), also conducted finite element analysis on both the moonie and cymbal end cap design. However, Tressler’s work focused on resonance frequency design of such devices. This work showed how the different end cap dimensions, such as the cap thickness, diameter, and cavity depth could be manipulated in order to control the ultrasonic cap resonance frequency. Tressler conducted both

in-air and in-water experiments which matched well with calculated data.

Kim [26], et al (2004), investigated the use of Soft PZT, Hard PZT, and High-G PZT in energy harvesting design. The researchers placed a piezoelectric cymbal energy harvester on a shaker and loaded the device with an 85g payload. The energy harvester was then base loaded with a cyclic  $7.8N$  force at  $100Hz$ . The results showed that the High-G PZT gave a voltage peak of  $374V$ , while the Hard PZT and Soft PZT gave  $260V$  and  $178V$  respectively. The results showed that in order to obtain maximum voltage from a piezoelectric material, the product of the effective piezoelectric field constant,  $d_{eff}$ , and the piezoelectric voltage constant,  $g_{eff}$ , should be maximized. As a result, Kim et al concluded that the High-G PZT material was best suited for energy harvesting applications.

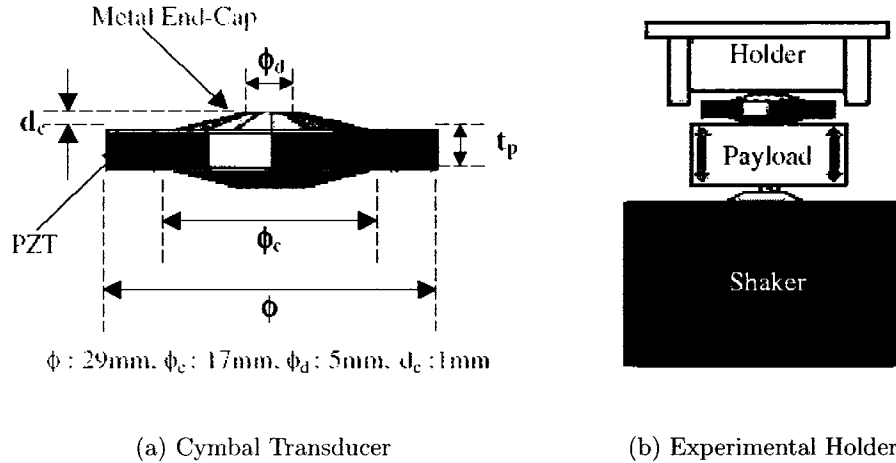


Figure 2-6: Diagram of (a) dimensions of the cymbal transducer and (b) designed holder for a cymbal transducer [26]

In addition, the work stated that the  $d_{eff}$  value of the piezoelectric material could be amplified significantly by the use of cymbal end caps. In fact, the cymbal end cap design has the advantage of combining both the  $d_{33}$  contributions with the amplified  $d_{31}$  contributions in order to create a very large  $d_{eff}$ . This large value of  $d_{eff}$  is given by the equation  $d_{eff} = d_{33} - Ad_{31}$ , where A is the amplification factor. The negative

sign is used to negate the conventional negative value of  $d_{31}$ . The amplification factor can be very large, in the range of 10–100, depending on the design of the end caps. The research showed that both the cavity depth and cavity diameter play a large role in the amplification factor as well as the resonance frequency of the device. The researchers further tested the High-G transducer and concluded that a 29mm diameter by 1mm thick piezo could produce 39mW of power when excited by the above mentioned forces. Figure 2-6 shows the cymbal transducer and experimental setup used by the authors.

Deng [27], et al (2004), also developed a cymbal energy harvester for use in low frequency environments. However, the cymbal fabricated in this study was designed to vibrate at its resonance frequency. This had the advantage of a reduced mass size that still allowed the cymbal energy harvester to achieve significant power increases. The research in this area was very successful, as the conversion efficiency claimed in the journal is over 50%. However, the Deng realized that in most applications, the exact resonance frequency is either changing or unknown. Deviations from the resonance frequency result in catastrophic power losses. To counteract this, Deng proposed a two degree of freedom system with two cymbal energy harvesters placed in series. This would broaden the range of frequencies that would excite the device. The journal discusses a mechanical model of The end caps of both cymbals are adjusted dimensionally to control the mechanical spring constants,  $K_1$  and  $K_2$ . The result of such a design is a much broader frequency spectrum.

# Chapter 3

## Design Investigation

A cantilever beam is a very compliant structure when used in a bending mode. As a result, designing for low resonance frequencies is not difficult. However, cantilever beams often suffer from highly localized mechanical-to-electrical energy conversion due to a non-uniform distribution of the deformation. In contrast, cymbal energy harvesters feature a uniform stress distribution, but designing for low resonance frequencies can prove to be quite difficult. In order to find a compromise between the two designs, a third energy harvester design is proposed. This design will be referred to as a *Carriage Spring* energy harvester and is shown in Figure 3-1. The main objective of this design is to combine both the low resonant frequency characteristics of a cantilever with the high mechanical-to-electrical conversion ratio of the cymbal design. The low resonance is achieved in a cantilever by allowing for a long, slender design while the high mechanical-to-electrical conversion of a cymbal design is achieved through the use of end caps. By designing appropriate rectangular end caps to fit on a long, slender section of piezoelectric material, it is hypothesized that a carriage spring design will produce a very efficient low frequency energy harvester. This design will be thoroughly investigated and compared to the other two types of piezoelectric energy harvesters in the sections to follow.

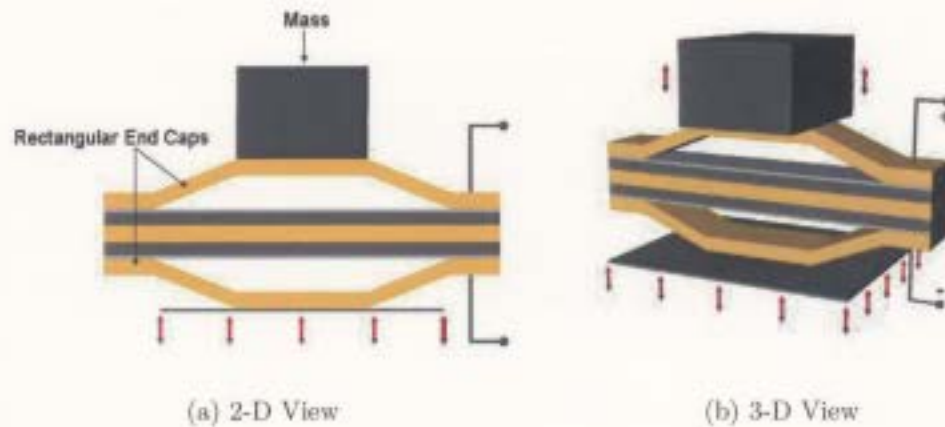


Figure 3-1: Piezoelectric carriage spring energy harvester shown in a (a) 2-D view and (b) 3-D view

### 3.1 Modeling in ANSYS

The Ansys [28] computer program is a multipurpose finite element program which is used to solve several classes of engineering problems. The analysis capabilities of Ansys include the ability to solve static and dynamic structural problems, steady-state and transient heat transfer problems, mode-frequency and buckling eigenvalue problems, static or time-varying magnetic analysis, piezoelectric analysis, and numerous other types of field and coupled-field applications. The Ansys program has been in commercial use since 1970, and has been used extensively in the aerospace, automotive, construction, electronic, energy services, manufacturing, nuclear, plastics, oil, and steel industries. In addition, many consulting firms and hundreds of universities use Ansys for analysis, research, and educational use.

The Ansys element library contains more than sixty elements for static and dynamic analysis, over twenty for heat transfer analysis, and includes numerous magnetic, piezoelectric, and special purpose elements. This variety of elements allows the Ansys program to analyze 2-D and 3-D frame structures, piping systems, 2-D plane and axisymmetric solids, 3-D solids, flat plates, axisymmetric and 3-D shells and nonlinear problems including contact (interfaces) and cables.

The input data for an Ansys analysis are normally prepared using a preprocessor. The general preprocessor (PREP7) contains the solid modeling and mesh generation capabilities, and is also used to define the geometric properties, material properties, constraints, and loads. The analysis results are reviewed using postprocessors, which have the ability to display distorted geometries, stress and strain contours, flow fields, safety factor contours, contours of potential field results (thermal, electric, magnetic), vector field displays mode shapes and time history graphs. A graphical user interface is available throughout the program, although writing script or batch files is the method of choice for most users.

Piezoelectrics are modeled in Ansys using a method known as coupled-field analysis. Coupled-field analysis allows one to couple the mechanical and electrical effects of a system into one set of compatible finite element equations. By using this method, a piezoelectric structure can be modeled either statically or dynamically in Ansys to determine *both* its mechanical and electrical characteristics. The sections below outline the procedures used to write a script to statically and dynamically model various piezoelectric structures in Ansys.

### **3.1.1 Ansys Preprocessing**

The first step in Ansys modeling is to enter the preprocessor (PREP7) and define the variables of interest that will be used throughout the script. Defining various dimension variables allows one to dynamically alter the size and shape of the structure under test at only one place in the code. This makes modifying and testing different designs very quick and simple. After defining the user variables, the coordinate systems are defined and the geometry of the structure is laid out. This is normally achieved by drawing keypoints in order to create lines. Once the lines are created, areas can be constructed to segregate the various sections of the structure to be meshed in a later step. For a cantilever beam, the separate areas are the top and bottom piezoelectric layer, the shim, and the mass. A cymbal design or carriage spring

will have two additional areas for the top and bottom end caps. Once the appropriate areas are glued (rigidly attached) together in Ansys, the geometry is complete. It is worthwhile to note that although Ansys does have 3-D capabilities, modeling simple structures in 2-D is preferred to lower the element count and speed up simulation time. As a result, all 3-D structures discussed in this thesis are modeled via their 2-D Ansys equivalent.

### 3.1.2 Element Selection

The next step is to select the finite element that will be used in order to model the energy harvester. The element chosen to model the piezoelectric material was the *plane223* coupled-field element. The *plane223* element is a 2-D solid element with structural, thermal, electrical, thermoelectric, piezoresistive, and piezoelectric capabilities. The element has eight nodes with up to three degrees of freedom per node. The main reason for choosing this element is for its piezoelectric and mechanical capabilities. The *plane223* element allows for the analysis of many structural effects, such as stress and strain, but also has the capability to couple these effects to an equivalent electrical voltage. In addition, the element has axisymmetric capabilities which is useful for modeling a cylindrical cymbal energy harvesters. Both cantilever beams and carriage spring generators make use of the plane stress option of the *plane223* element instead.

Although this element is perfect for mechanical-to-electrical coupling, it is also a very good mechanical modeling element. Consequently, this element is also used to model the mass, center shim, and end caps of the various energy harvester designs as well. The only difference is that the *plane223* element used for these sections contains different material constants and is void of any piezoelectric capabilities.

### 3.1.3 Material Selection

The end caps and center shim are made out of brass. There are two reasons for this selection. First, brass is a very strong, yet flexible material. This allows for energy harvester designs with a lowered resonance frequency than would be possible with a stronger material, such as steel. The second reason is that brass is a very good conductor of electricity and is easily solderable. This means that the end caps can be very easily soldered to the piezoelectric material and can double as electrodes.

The material selection for the mass is quite arbitrary as long as the mass value is correct. Therefore, the mass is modeled as a steel section with an exaggerated density. The reason for increasing the density is to make the physical mass size smaller in order to decrease the element count. In addition, a smaller mass allows the figures to be positioned more appropriately for display purposes. This modification has no impact on the results obtained from Ansys.

Selecting the appropriate piezoelectric material, however, is a little more involved. There are four main piezoelectric material properties that are important when choosing a specific piezoelectric material. The strain coefficient ( $d$ ) relates the strain to the electric field and the coupling coefficient ( $k$ ) is an indication of the materials ability to convert mechanical energy to electrical energy or vice versa [2]. It is normally desirable to select materials with high strain and coupling coefficients to maximize their energy conversion potential. The elastic modulus ( $Y$ ) of a material affects the stiffness of the energy harvester design. When designing for low resonance frequencies, as is normally the case, this value is best kept as low as possible. Finally, a higher dielectric constant ( $K^T$ ) is also preferred as it lowers the source impedance of the generator [2]. A low source impedance is desirable when designing interface circuitry to lower the voltage necessary for maximum power output. Table 3.1 shows the various piezoelectric properties associated with different piezoelectric materials.

The elastic modulus of PVDF is very low, which makes this material useful for sensor and actuator designs in which low resonance is desirable. However, the poor

Property	Units	PVDF	PZT-5A	PZT-5H	PZN-PT
Strain coefficient ( $d_{31}$ )	$10^{-12}m/V$	20	190	320	1000
Strain coefficient ( $d_{33}$ )	$10^{-12}m/V$	30	390	650	2000
Coupling coefficient ( $k_{31}$ )	$CV/Nm$	0.11	0.35	0.44	0.51
Coupling coefficient ( $k_{33}$ )	$CV/Nm$	0.16	0.72	0.75	0.91
Elastic modulus ( $Y$ )	$10^{10}N/m^2$	0.12	6.6	6.2	2.2
Dielectric constant ( $K^T$ )	$\epsilon/\epsilon_0$	12	1800	3800	7500

Table 3.1: Comparison of different piezoelectric materials [29], [30], [31]

energy conversion shown by the strain and coupling coefficients make it quite impractical for energy harvesting. PZT materials are the most commonly used piezoelectric material. PZT-5A is very durable and is quite insensitive to temperature variations; however, PZT-5H has a slightly lower elastic modulus and a much higher dielectric constant. In addition, PZT-5H has a much higher strain and coupling coefficient than PZT-5A. PZN-PT is a new piezoceramic that is very expensive and quite new to the market. This material has extremely good electrical and mechanical characteristics that make it a very promising research topic for energy harvesters in the future. Unfortunately, due to economic cost and availability constraints, it was decided that a PZT-5H piezoceramic purchased from Piezo Systems Incorporated would be the best material in which to model and construct an energy harvester.

### 3.1.4 Defining Material Constants

Table 3.2 gives the material constants used for Ansys modeling. The data for the piezoelectric properties were obtained from the manufacturer, Piezo Systems Inc., with a tolerance of  $\pm 10\%$ . However, data denoted by a \* symbol were not obtainable from the manufacturer and was therefore completed by using generic PZT-5H data found in [32].

The data for the brass and steel material was easily entered in Ansys using standard material property commands. However, entering the material properties to accurately model the piezoelectric layers involves appropriately initializing the piezoelectric matrices. The first piezoelectric matrix to be assembled is the piezoelectric

Property	Units	PZT-5A	Brass	Steel
Compliance ( $s_{11}^E$ )	$10^{-12}ms^2/kg$	16.1	7.69	5.0
Compliance ( $s_{33}^E$ )	$10^{-12}ms^2/kg$	20.0	7.69	5.0
Compliance ( $s_{12}^E$ )	$10^{-12}ms^2/kg$	-4.78*	-	-
Compliance ( $s_{13}^E$ )	$10^{-12}ms^2/kg$	-8.45*	-	-
Compliance ( $s_{44}^E$ )	$10^{-12}ms^2/kg$	43.5*	-	-
Strain coefficient ( $d_{31}$ )	$10^{-12}m/V$	-320	-	-
Strain coefficient ( $d_{33}$ )	$10^{-12}m/V$	650	-	-
Strain coefficient ( $d_{15}$ )	$10^{-12}m/V$	741*	-	-
Dielectric constant ( $K_{11}^T$ )	$\epsilon_{11}/\epsilon_0$	3130*	-	-
Dielectric constant ( $K_{33}^T$ )	$\epsilon_{33}/\epsilon_0$	3800	-	-
Density ( $\rho$ )	$kg/m^3$	7800	8400	7850

Table 3.2: Material constants used for Ansys modeling

compliance matrix evaluated at constant strain,  $[s^E]$ . Ansys allows the user to enter either a compliance matrix or a stiffness matrix,  $[s^E]^{-1}$  and is purely a matter of preference. For the Ansys program written in Appendix A, a stiffness matrix is entered in the standard symmetric form outlined in [33]. The next step is to set up the piezoelectric matrix of strain coefficients,  $[d]$ . The user has the option of entering this matrix as either strain or stress per electric field. The stress per electric field option is utilized in Appendix A. Finally, the dielectric constants in the X, Y, and Z directions must be defined.

Constructing any one of the above mentioned matrices in Ansys can be quite complicated as Ansys does not necessarily follow the exact standard form outlined in most literature. For an excellent discussion on how to convert standard piezoelectric data into appropriate Ansys matrices, please refer to [32].

### 3.1.5 Meshing

The next step in the modeling of piezoelectric energy harvesters involves meshing. Meshing allows Ansys to break down the structure into thousands of small plane223 elements. The reaction of each element to any given disturbance can then be compiled into large matrices using standard finite element techniques. The element sizes used in the modeled piezoelectric energy harvester range from 70-100 $\mu m$ , depending on

the material. When meshing piezoelectric material it is very important to use the appropriate coordinate system. Defining two local coordinate systems offset by 180 degrees allows the user to control the poling direction of the piezoelectric layer easily. This technique is quite convenient when changing from the series to parallel-poled energy harvesters discussed in Section 3.2.2.

### **3.1.6 Solving the Problem**

Ansys has the capability to perform static, modal, harmonic, and transient solutions. In order to utilize the static analysis, a load must be applied to some part of the structure. For the maximum voltage investigation discussed in Section 3.2.3, a small displacement is applied to the top of the structures and the output voltage is noted. For the mechanical investigation in Section 3.2.4, the modal analysis option, which utilizes the Block Lanczos method, is used to determine the first resonance frequency of the different energy harvester structures and configurations.

### **3.1.7 Analysing the Results**

The final step in the Ansys investigation is to view the results. This is done through the use of the general Ansys postprocessor (POST1). This Ansys postprocessor has the ability to graphically display and animate the motion and distribution of a variety of mechanical and electrical responses. The POST1 processor was used to create the various color-mapped graphical Ansys figures displayed throughout this thesis.

## 3.2 Energy Harvester Design Comparison

Piezoelectric energy harvesters can be classified by the way in which they stress a section of piezoelectric material. Typically, cantilever energy harvesters are referred to as *bending* generators whereas cymbal and carriage spring energy harvesters are referred to as *extension* generators. Due to the fact that a cymbal and carriage spring generator stress piezoelectric material in exactly the same manner, by extending it, it can be assumed that both of their 2-D (thin slice) piezoelectric voltage distributions are identical. Consequently, when discussing electrical phenomena, such as piezoelectric poling and mechanical-to-electrical energy conversion, it is convenient to adopt this nomenclature and group both cymbal and carriage spring designs together. However, when discussing mechanical phenomena, such as resonance, the three designs are best compared separately.

### 3.2.1 Piezoelectric Layering Selection

As mentioned in previous sections, piezoelectric energy harvesters can have  $n$  layers of piezoelectric material that may or may not be separated by a metallic shim. Piezoelectric materials are normally very brittle and are quite difficult to work with. Adding a thin metallic shim provides mechanical strength as well as extends the lifetime of the piezoelectric material. However, adding a shim does increase the resonance frequency significantly. Depending on the application, the designer must weigh the tradeoffs of lowered resonance with structural strength of different styles of energy harvesters. A center shim is almost always used with a cantilever beam, but hardly ever used with a cymbal transducer. This is because a cantilever beam, being a very soft structure, needs extra support in order to accommodate the required mass necessary to stress the piezoelectric material. In addition, bending a thin, brittle piezoelectric material without producing cracks is very challenging. A cymbal structure, on the other hand, is normally quite rigid due to the end caps. As a result, the end caps themselves can

### 3.2.2 Poling Configurations

There are two main poling orientations for dual-layered piezoelectric materials. The first is to have both the top and bottom layer poled in the same direction. This configuration is used for connecting a bending generator for parallel operation and an extension generator for series operation. The second is to have the top and bottom layer poled in opposite directions. This is used for connecting a bending generator in series and an extension generator in parallel. Figure 3-2 shows the different poling configurations for both bending and extending generators. The direction of poling for each piezoelectric layer is shown by the arrows.

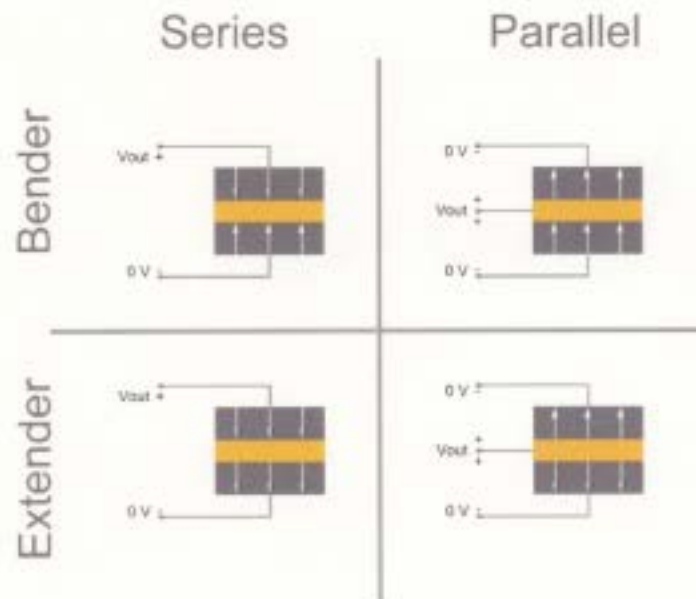


Figure 3-2: Poling directions for series and parallel extender and bender designs

The reason for the reversal of electrical connections for the two poling orientations is that when a cantilever beam bends, the top layer extends while the bottom layer simultaneously contracts. These two actions produce two equal but oppositely oriented voltages if the layers are oriented in the same direction. Therefore, a center tap can be used to extrude the low voltage level from the center shim. Figure 3-3

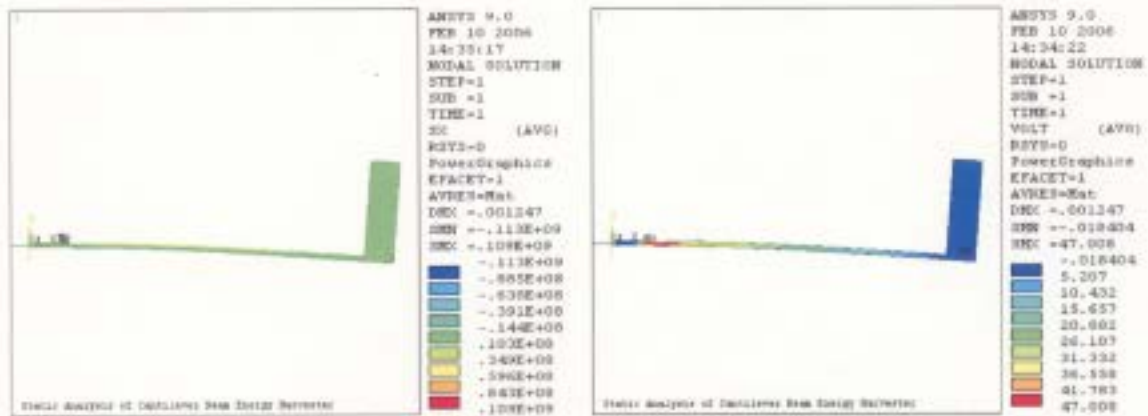
shows the horizontal stress and corresponding voltage output of a bending generator wired for parallel operation. When a cymbal or carriage spring generator extends, both the top and bottom layer extend together. Therefore, two oppositely poled layers are needed in order to extract the center tap voltage from the center shim. Figure 3-4 shows the horizontal stress and corresponding voltage output of an extending generator wired for parallel operation.

### 3.2.3 Mechanical-to-Electrical Power Conversion

The generators shown in Figures 3-3 and 3-4 were both constructed of identically sized and shaped sections of piezoelectric material with identical material properties. To keep consistent, the same active piezoelectric region was maintained in both designs. To clarify, the extension generator sacrifices two  $2.5mm$  sections of active piezoelectric regions on each side of the piezoelectric material in order to attach the end caps. To stay consistent, the bending generator was anchored with a  $2.5mm$  clamp and the mass was positioned to use  $2.5mm$  of piezoelectric space. Because neither one of these  $2.5mm$  sections experiences a stress in the X-direction, no voltage is produced. Therefore, both the extending and bending generator have the exact same amount of usable piezoelectric material left over with which to generate electricity.

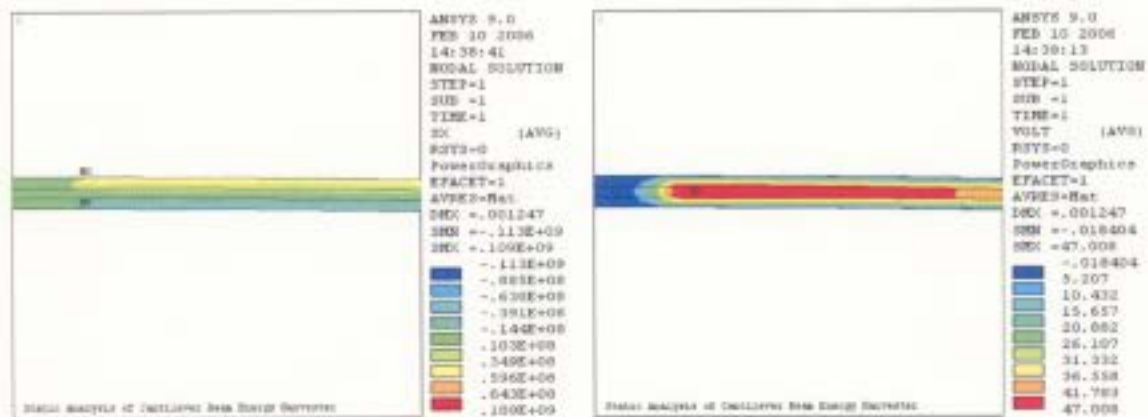
Both generators were then excited with a static force on their mass to simulate the movement that would be experienced in a transient vibration scenario. The force was adjusted for both such that no point on the piezoelectric layer experienced a strain larger than the manufacturers' suggested maximum strain of  $500\mu\epsilon$ . As can easily be seen in Figure 3-3, the stress in the X-direction of a cantilever beam is not constant. The stress is greatest at the clamping point of the bending generator and it is weakest at the point closest to the mass. Because voltage output is directly proportional to stress, as shown in Equation 1.13, the voltage drops significantly along the length of the beam. Historically, researchers using cantilever beams for energy harvesting overcame this problem by placing the top and bottom electrodes only on the section of

the piezoelectric material near the clamp. Because a piezoelectric material produces power only in the region that is covered by an electrode, the voltage was kept high while the rest of the piezoelectric material was used simply for mechanical purposes. Obviously, this is a less than optimal design as only a fraction of the piezoelectric material is being used for energy harvesting.



(a) X-stress distribution

(b) Voltage distribution

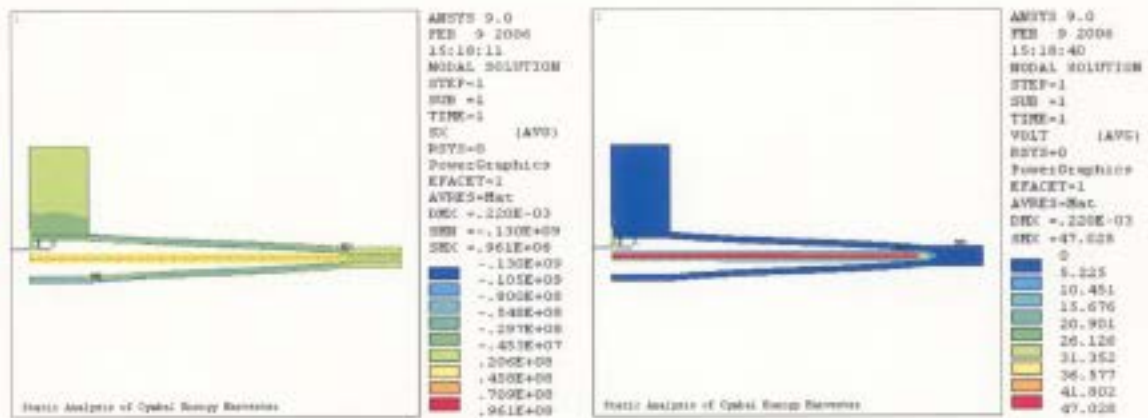


(c) X-stress distribution

(d) Voltage distribution

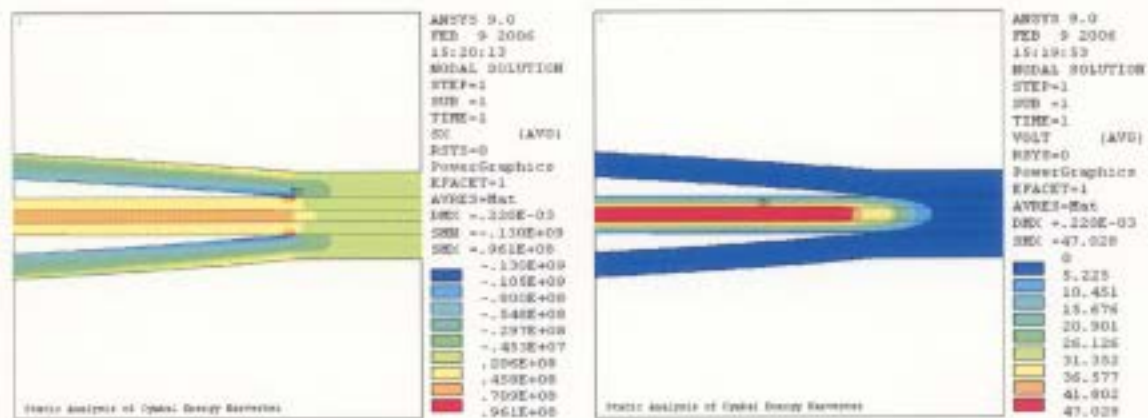
Figure 3-3: Bending generator (a) X-stress distribution, (b) voltage distribution, (c) zoomed X-stress distribution (d) zoomed voltage distribution

The extending generator, shown in Figure 3-4, has a constant stress distribution in the X-direction. This leads to a very consistent voltage distribution throughout the entire piezoelectric layer. As a result, 100% of the useable piezoelectric material is being utilized for energy harvesting.



(a) X-stress distribution

(b) Voltage distribution



(c) X-stress distribution

(d) Voltage distribution

Figure 3-4: Extending generator (a) X-stress distribution, (b) voltage distribution, (c) zoomed X-stress distribution (d) zoomed voltage distribution

In addition, because the stress is constant, the device can easily be designed to stress at its maximum where each molecule of piezoelectric material is producing a very large amount of electrical power. The voltage distribution for both the bender and extender generator are given in Figure 3-5 as a function of the percentage distance from one end of the piezoelectric material to the other. The average voltage produced by the bending generator is only 22.8V. This is less than one half of the 47V produced by the extending generator. However, because electrical power is proportional to the square of the voltage, as in Equation 1.14, the potential power produced by this particular bending generator will be only one quarter of the power produced by the extending generator assuming that the internal resistance remains essentially the same.

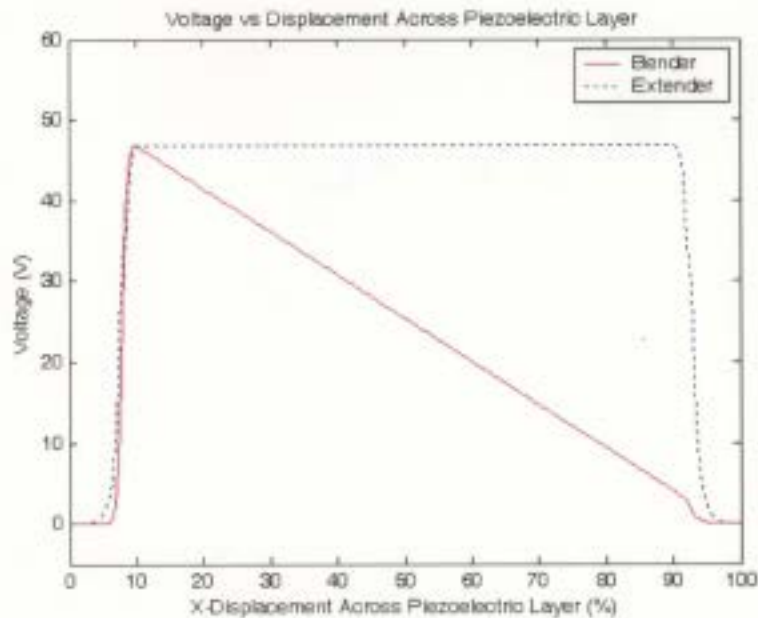


Figure 3-5: Comparison of extender vs. bender voltage distributions

### 3.2.4 Resonance Frequency Design

Figure 3-6 shows how the resonance frequencies of the three different energy harvester structures are affected by the length of the piezoelectric material being used. The three different energy configurations had their length-to-width ratio adjusted in order to maintain a constant piezoelectric surface area throughout the investigation. It can be seen that the cantilever beam easily obtains the lowest resonance frequency; however, there is not a very large range over which the resonance frequency can be adjusted by adjusting the length of the energy harvester.

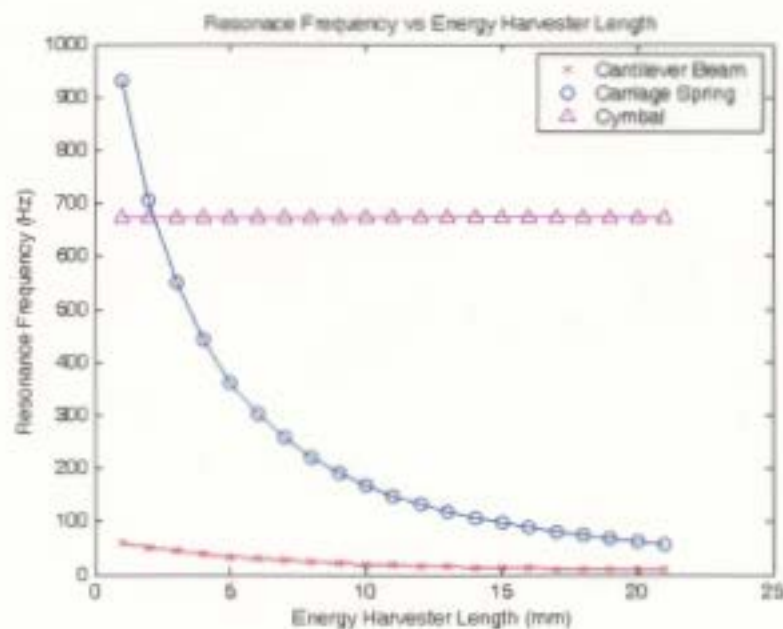


Figure 3-6: Resonance frequency comparison of different energy harvester designs

To investigate the extending generators, the cap height and thickness were maintained at constant values in order to observe how a change in piezo length only affected the resonances. It should be noted that as the piezo length extended, the cap length also extended proportionally. The cymbal design appears as a straight line in the figure. This is because a cymbal, by definition, is of a cylindrical shape. Therefore, there is only one length-to-width ratio that will result in the surface area common to

the other two designs. In fact, the surface area,  $A$ , is instead dependent on only the radius,  $r$ , by the relation  $A = \pi r^2$ . Consequently, the cymbal only has one resonance frequency for the given piezo surface area. Also, this frequency is quite high when compared to the others as a cymbal is an extremely stiff structure. The carriage spring, on the other hand, had a wide range of resonance frequencies obtainable by simply designing for a longer, more slender structure. Although the carriage spring cannot obtain low resonances as easily as the cantilever, it does have the ability to have a highly adjustable resonance frequency by simply lowering the stiffness of the structure by adjusting the piezo and cap length. However, given the correct micromachining fabrication equipment, it is believed that resonances frequencies equivalent to those of the cantilever beam could be achieved by simply lowering the cap height and thickness of the carriage spring energy harvester.

### 3.2.5 Conclusions Regarding Energy Harvesters

It would appear that there are three different criteria which will determine the proper energy harvester design to use in any given situation. These criteria are mechanical-to-electrical conversion efficiency, resonance frequency level, and durability. When high mechanical-to-electrical conversion efficiency is required, the best device would be an extending generator. Both the cymbal transducer and the carriage spring design have the exact same conversion capabilities. When a very low resonance frequency is required, a cantilever beam configuration would most likely be best suited. However, a carriage spring also offers the ability to have a low resonance frequency, with the added benefit of excellent mechanical-to-electrical conversion properties. Finally, for high frequencies and environments with high acceleration levels, the cymbal would be by far the stiffest and most durable structure. The next best structure would be the carriage spring, and the worst structure would be the cantilever beam. In fact, many cantilever beam energy harvesters have been proven to produce small cracks at cyclic frequencies as low as  $50\text{--}100\text{Hz}$  [26].

No matter what the environment, the carriage spring design is quite promising. This design is a solid compromise between the low resonance properties of a cantilever and the high electrical efficiencies of the cymbal and definitely warrants further investigation. As a result, the thesis will now change focus from investigating different energy harvester structures to taking a closer look at the carriage spring design. The following sections will thoroughly investigate the properties of this previously unexplored design.

### 3.3 Detailed Carriage Spring Resonance Investigation via DOE

Design of Experiments, commonly referred to as DOE, is a methodology for systematically applying statistics to experimentation [34]. The main advantage to DOE is that it helps researchers develop mathematical models that predicts how input values *interact* to create output variables or responses in a process or system. One specific type of DOE is Response Surface Methodology (RSM).

RSM is a collection of mathematical and statistical techniques that are useful for the modeling and analysis of problems in which a response of interest is influenced by several variables and the objective is to optimize the response [34]. Every experiment begins with some type of conjecture, or hypothesis, which motivates the experiment. Next, the appropriate factors and levels, also know as treatments, that will be used in the experiment must be selected. A factor normally refers to a variable which is chosen in an experiment, while the level refers to the number of different values selected for each factor. The nomenclature common for describing such a setup is  $a^k$ , where  $a$  is the number of levels and  $k$  is the number of factors. The next step in the procedure is to carry out the experiment and collect the results. Once the results are collected the analysis of the data can begin.

The first process in the statistical analysis of the data is to complete an Analysis of Variance (ANOVA) table. This table uses the statistical techniques outlined in Montgomery [34] to determine which factors and which interaction between factors are statistically significant. The primary objective of an ANOVA analysis is to test the hypotheses about the equality of the treatment means by partitioning the total variability in the response variable into components that are consistent with a model for the experiment. Once the ANOVA table is finalized, an equation can be developed to predict the response of changing the values of the different factors. The process used to develop these equations is known as regression analysis. The analysis is

usually completed with some form of optimization in which factors can be chosen to either maximize, minimize, or target a response.

### 3.3.1 Setting up the Problem

An experiment is set up in order to develop insight into the proposed phenomena. For this study, the experiment consisted of mathematically modeling the energy harvester in the finite element software package Ansys. A modal analysis using the Block Lanczos method was utilized by Ansys in order to determine the first resonance frequency of the specific treatment level. The dimensional values outlined in Table 3.3 were then changed in accordance with the treatments suggested by the DOE software program Design Expert [35]. The objective for this experiment is to gain insight into the effect of changing different end cap parameters on the first resonance frequency of the energy harvester. Therefore, in order to keep the experiment simplified, the piezo size and thickness were held constant throughout the experiment. In fact, the piezoelectric material dimensions and material are exactly the same as those previously used in past investigations within this document.

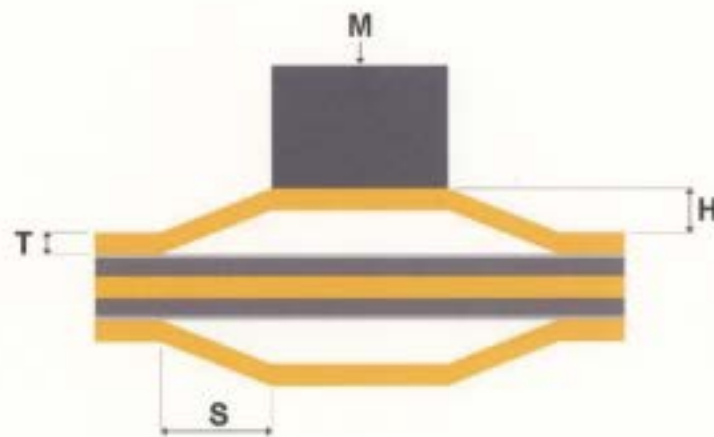


Figure 3-7: Cross-sectional view of cymbal energy harvester

Factor	Symbol	Units	Level 1	Level 2
Mass	M	<i>g</i>	50	130
Cap Height	H	<i>mm</i>	0.5	2.0
Cap Thickness	T	<i>mm</i>	0.25	0.4
Surface Length	S	<i>mm</i>	7.5	11

Table 3.3: Levels, factors, and ranges for  $2^4$  design

The specific DOE analysis utilized for this experiment was a  $2^4$  face-centered RSM Central Composite Design (CCD). A CCD is similar to other RSM designs in which runs are completed at different factor levels. However, a CCD also contains alpha points which normally extend beyond the range of the factor levels in order to test for curvature and to fit a second order model. A face-centered design is chosen for this experiment in which the alpha values are located at the *midpoint* of the different levels. This type of design has the advantage of increased accuracy for the range of levels under test. The experiment conducted for the initial trial included 25 runs with only one center point. The appropriate factors and levels are shown in Table 3.3 and the corresponding labels are shown in Figure 3-7.

### 3.3.2 Sum of Squares

The Sequential Model Sum of Squares table is developed by the DOE software to determine what model is best suited to describe the output. The objective is to choose the highest order polynomial where additional terms are significant and not aliased. Aliasing refers to combining phenomena together such that the experimenter is not sure what effect actually caused the output. This occurs when the CCD model does not have enough runs to support the model that it is attempting to match to the output. This phenomena is evident in the cubic model shown in Table 3.4. Consequently, the highest unaliased model that is statistically significant is the Quadratic model with a p-value much less than 0.05. Selecting a model with a p-value less than 0.05 is a typical way to prove statistical significance. In other words, the chance of wrongfully rejecting the null hypothesis is less than 5%.

Source	Sum of Squares	df	Mean Square	F Value	p-value Prob > F	
Mean	4114.3	1	4114.3			
Linear	265.16	4	66.29	165.84	< 0.0001	
2 Factor Interactions	6.47	6	1.08	9.91	0.0002	
Quadratic	1.34	4	0.34	18.45	0.0001	Suggested
Cubic	0.18	8	0.023	110.48	0.0090	Aliased
Residual	0.0004104	2	0.0002052			
Total	4387.46	25	175.5			

Table 3.4: Sequential model sum of squares

### 3.3.3 ANOVA Analysis

The next step is to analyze the Analysis of Variance (ANOVA) table. The key objective here is to find effects where the p-value is less than 0.05 to be included in the model. If any of the effects or interactions are deemed insignificant, those effects must be removed from the model and the analysis must be redone. Luckily, Design Expert makes this quite a simple process. Table 3.5 shows the ANOVA table after all insignificant effects are removed. It can easily be seen that all effects shown in this table have a p-value less than 0.05.

One thing to notice is that the sum of squares value for the cap height is very large compared to the sum of squares of the other variables. This means that cap height has the largest effect on the system. The mass and surface length have a moderate effect on the system, while the cap thickness has very little effect on the system.

The adjusted  $R^2$  value given in the analysis states that 99.82% of the variability in the resonance frequency is explained by the mass, cap height, cap thickness and surface length. The most important of all data given by the ANOVA analysis is the predictability of the model given new data. In this case, the predicted  $R^2$ , based on the PRESS (Predicted Error Sum of Squares) value, is excellent at 99.61%. However, the only way to test this for certain is to try new runs using different values than those previously selected in the DOE experiment in order to verify the model. In addition, in order for the model to be considered statistically significant, it must pass a series

Source	Sum of Squares	df	Mean Square	F Value	p-value Prob > F	
Model	272.91	12	22.74	1106.34	< 0.0001	significant
A-Mass	42.29	1	42.29	2057.37	< 0.0001	
B-Height	159.38	1	159.38	7753.13	< 0.0001	
C-Thickness	9.81	1	9.81	477.31	< 0.0001	
D-Surface	53.68	1	53.68	2611.37	< 0.0001	
$A^2$	0.42	1	0.42	20.59	0.0007	
$D^2$	0.12	1	0.12	5.76	0.0335	
AB	2.00	1	2.00	97.39	< 0.0001	
AC	0.13	1	0.13	6.25	0.0279	
AD	0.67	1	0.67	32.69	< 0.0001	
BC	1.32	1	1.32	64.28	< 0.0001	
BD	2.91	1	2.91	106.62	< 0.0001	
CD	0.16	1	0.16	7.58	0.0175	
Residual	0.25	12	0.021			
Cor Total	273.16	24				

Table 3.5: ANOVA table

of statistical tests which are normally conducted by means of diagnostic plots. The diagnostic plots relevant to this study are shown and explained in Appendix B

### 3.3.4 Results

After the ANOVA analysis is complete, the path of steepest ascent method is utilized by Design Expert to determine an equation for the resonance frequency. The equation produced by Design Expert is

$$f_{res} = \left( \begin{array}{l} 16.69732 - 0.081827M + 9.29751H + 25.8759T - 1.81475S \\ +0.000227M^2 + 0.062775S^2 - 0.011791MH - 0.029879MT \\ +0.002928MS - 5.10896HT - 0.28199HS - 0.75205TS \end{array} \right)^2 \quad (3.1)$$

Now that an equation has been developed to describe how the mass, cap height, cap thickness, and surface length affect the resonance frequency of the energy harvester, various interaction graphs can be created to see how these dimensional variables interact to produce different resonance frequencies. Figure 3-8 shows a 2-Dimensional and 3-Dimensional view of how the resonance frequency changes with a changing mass and cap height. In Figure 3-8 (a), the red line represents the cap height at its high level,  $2mm$ , while the black line represents the cap height at its low level,  $0.5mm$ . It should be noted that these graphs maintain a constant cap thickness and surface length of  $0.33mm$  and  $9.25mm$  respectively. These values are chosen to be the midpoint values of the ranges selected in Table 3.3.

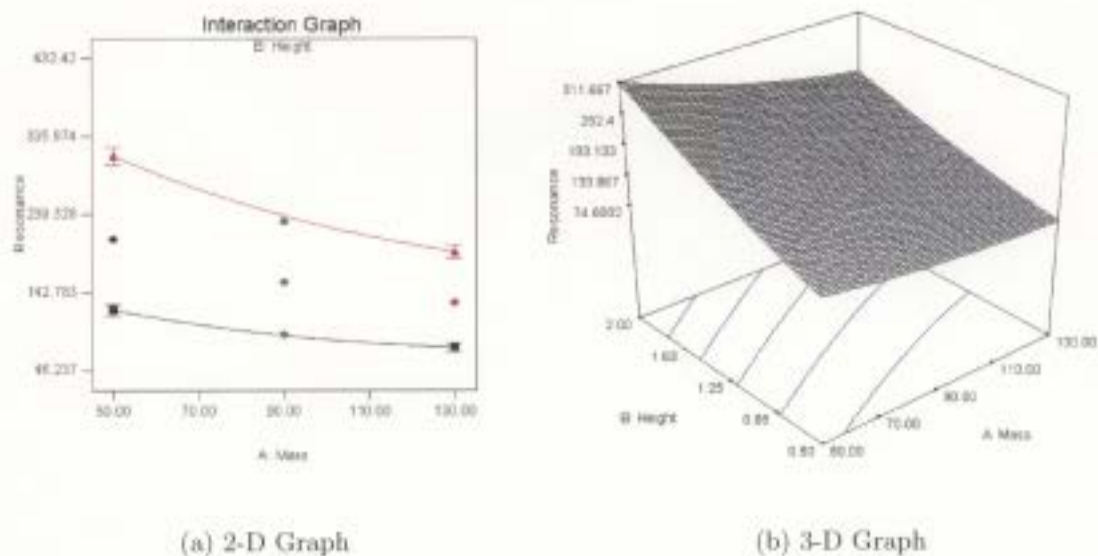


Figure 3-8: Mass and cap height vs. resonance frequency via (a) 2-D graph and (b) 3-D graph

It is easily observed that for any given cap height, an increase in mass results in a decrease of resonance frequency. However, by observing Figure 3-8 (a) more closely, it is evident that the high and low level lines are not parallel. This implies that an interaction is occurring. It is quite evident from the graph that the cap height plays

a more crucial role when the mass is low and less of a role when the mass is high. Another way to describe the phenomena would be to say that it is easier to control the resonance frequency of the energy harvester by adjusting the cap height when the mass is low. However, a tradeoff between the two exists as a device with a larger mass ultimately has a lower resonance frequency. Figure 3-8 (b) gives a view of the frequency response over the entire range of possible cap heights.

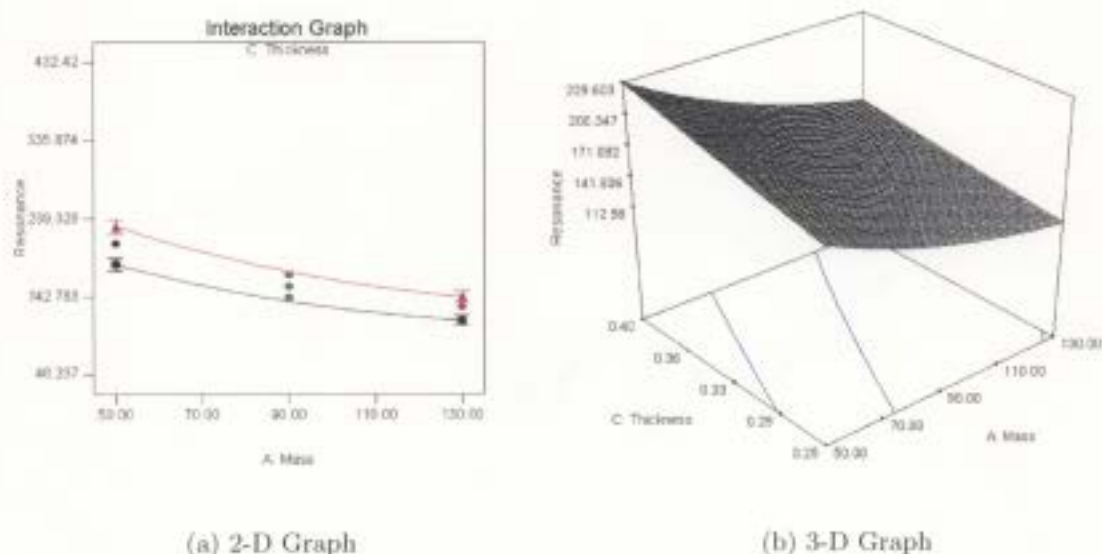


Figure 3-9: Mass and cap thickness vs. resonance frequency via (a) 2-D graph and (b) 3-D graph

Figure 3-9 shows how the resonance frequency is affected by changing the mass and cap thickness. The red line in Figure 3-9 (a) represents the cap thickness at its height level of  $0.4\text{mm}$ , while the black line shows the cap thickness at its low level of  $0.25\text{mm}$ . Once again, the other factors, the cap height and surface length, are kept at their midpoint values of  $1.25\text{mm}$  and  $9.25\text{mm}$  respectively. It is observed that a thinner cap ultimately produces a lower resonance frequency as there is only a slight interaction occurring in Figure 3-9 (a). However, once again there exists a tradeoff. Although a very thin cap is ideal, there is obviously a limit to how much force it

can withstand before it begins to buckle. Therefore there is a tradeoff between low frequency design through cap thickness and structural integrity.

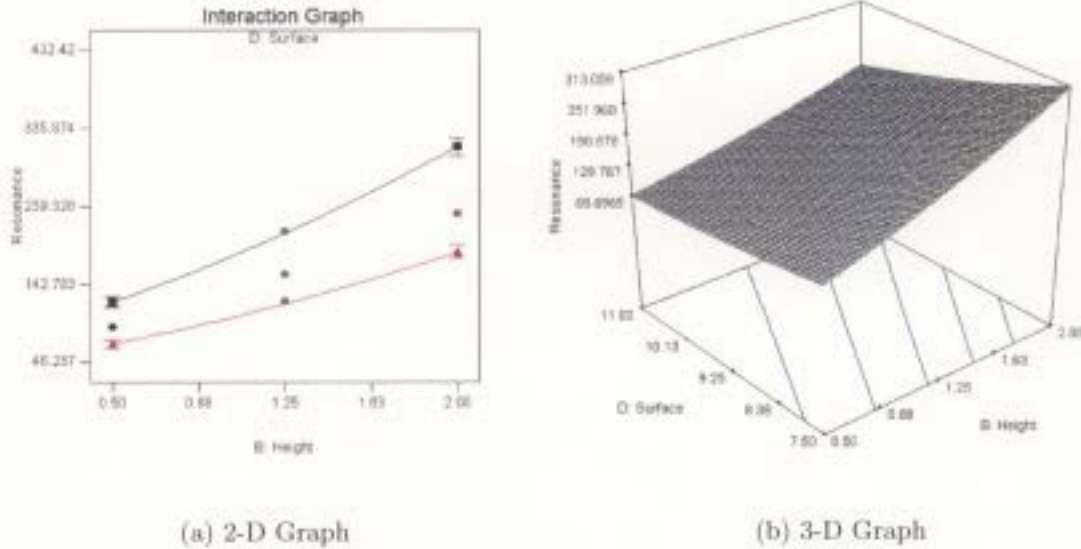


Figure 3-10: Surface length and cap height vs. resonance frequency via (a) 2-D graph and (b) 3-D graph

Figure 3-10 demonstrates the effect of surface length and cap height on the carriage spring resonance frequency. The red line in Figure 3-10 (a) shows the surface at 11mm, while the black line represents the surface length at 7.5mm. All other factors are held at their midpoint values of 90g and 0.33mm respectively for the mass and cap thickness. Figure 3-10 (a) shows a rather strong interaction between the cap height and surface length. For a small cap height, the surface length is less crucial than when the cap height is large. However, in either case, a larger surface area helps to decrease the resonance frequency of the device.

### 3.3.5 Optimization

After completing the analysis, the final step is to optimize based on the desired design criteria. Optimization can be performed in Design Expert to minimize or maximize a response, hit a target value, or hit a range of required responses based on a range of input values. Table 3.6 gives ten optimized possible designs in order to minimize the resonance frequency of the energy harvester given the ranges used in the experiment.

Num	Mass	Height	Thickness	Surface	Resonance	Desirability
1	134.52	0.50002	0.25000	11.000	46.608	0.99805
2	135.00	0.50000	0.25000	10.789	47.697	0.99239
3	134.01	0.50000	0.25000	10.620	48.690	0.98728
4	135.00	0.50003	0.26411	11.000	48.744	0.98700
5	104.47	0.50000	0.25000	11.000	50.254	0.97933
6	134.97	0.50000	0.25000	10.221	51.131	0.97493
7	98.810	0.50000	0.25000	10.998	51.624	0.97248
8	130.89	0.50000	0.28508	11.000	52.238	0.96943
9	134.94	0.50024	0.33476	11.000	60.228	0.93134
10	135.00	0.50000	0.37269	10.996	66.902	0.90142

Table 3.6: Optimized designs for lowest resonance frequency

Many times it is desirable to target a specific resonance frequency. Table 3.7 give ten optimized designs where the objective is to minimize the mass while maintaining a resonance frequency of  $100Hz$ . It should be noted that it is possible to extend the optimization outside of the ranges used for the experiment; however, there is no guarantee that the model will hold for such values.

Num	Mass	Height	Thickness	Surface	Resonance	Desirability
1	50.000	0.52408	0.25944	9.4113	100.00	1.0000
2	50.000	0.79134	0.25817	10.956	100.00	1.0000
3	50.000	0.51822	0.33019	10.669	100.00	1.0000
4	50.000	0.52090	0.25371	9.2923	100.00	1.0000
5	50.000	0.50577	0.34974	10.976	100.00	1.0000
6	50.000	0.50053	0.27738	9.5968	100.00	1.0000
7	50.000	0.53021	0.26012	9.4582	100.00	1.0000
8	50.000	0.50000	0.25000	8.6110	108.99	0.97941
9	50.000	0.50001	0.38913	10.959	110.78	0.97537
10	50.001	0.51799	0.25000	8.3621	115.84	0.96401

Table 3.7: Optimized designs for 100Hz resonance frequency with minimal mass

### 3.3.6 Conclusions Regarding DOE

In conclusion, it would appear that in order to minimize the resonance frequency of a carriage spring energy harvester, the designer should aim to make the mass large, the cap height small, the cap thickness small, and the surface length large. However, any energy harvester designer should take into consideration the physical limits of such a design. For example, the device should have enough clearance such that the piezoelectric element does not contact the end caps during operation. In addition, the structural integrity of the device should be considered, as a cap that is too thin with a surface area that is too large will almost always result in a buckle or may introduce new undesirable resonances into the system. No matter what the criterion or limits of design, one must always appreciate how the *interactions* between all these variables will affect both the resonance frequency as well as the structural integrity of the device. The resonance frequency equation of the carriage spring energy harvester as a function of mass, cap height, cap thickness, and surface length was shown to be

$$f_{res} = \left( \begin{array}{l} 16.69732 - 0.081827M + 9.29751H + 25.8759T - 1.81475S \\ +0.000227M^2 + 0.062775S^2 - 0.011791MH - 0.029879MT \\ +0.002928MS - 5.10896HT - 0.28199HS - 0.75205TS \end{array} \right)^2 \quad (3.2)$$

It should be noted that the goal of this chapter was to investigate the transducer design, identify critical parameters, and unearth sensitivities and cross-correlations that are of interest to future designers with large monetary resources and an interest in this field. Consequently, the design parameters used in the following chapter are chosen to coincide with typical off-the-shelf piezoelectric parameters provided by the manufacturer, instead of the optimal designs outlined in this chapter. Although the author realizes that the device in the next chapter will be sub optimal, it is still worthwhile to undertake such an investigation to produce a proof-of-concept device.

# Chapter 4

## Experimental Results

### 4.1 Prototype Design

A carriage spring prototype was fabricated in order to study the power producing potential of such a device. The piezoelectric material used in the prototype had a length of  $31.9\text{mm}$  and a width of  $6.4\text{mm}$ . The piezoelectric material was constructed from two layers of  $0.14\text{mm}$  thick PZT-5H sandwiched on top of a  $0.13\text{mm}$  thick brass center shim purchased from Piezo Systems Inc. Although, ideally, an energy harvester without a center shim would more easily obtain a lower resonance frequency, it was ultimately decided that a piezoelectric device with a center shim would provide more mechanical strength and reduce the risk of cracking the brittle ceramic piezo. The end caps were fabricated from two  $31.9 \times 6.4\text{mm}$  brass sheets of  $0.325\text{mm}$  thickness. The brass sheets were then carefully bent using a break and roll into the desired dimensions. Table 4.1 gives the dimensions for the end caps which are shown in Figure 4-1.

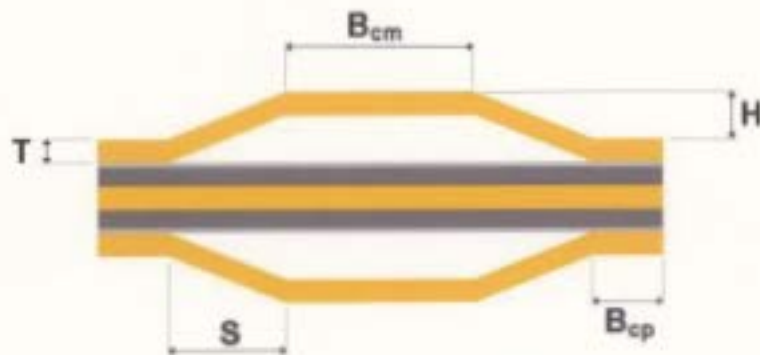


Figure 4-1: Experimental dimensions of carriage spring prototype

Dimension	Symbol	Units	Value
Cap Height	$H$	$mm$	1.36
Cap Thickness	$T$	$mm$	0.325
Surface Length	$S$	$mm$	10.9
Cap to Piezo Bond Length	$B_{cp}$	$mm$	2.5
Cap to Mass Bond Length	$B_{cm}$	$mm$	5

Table 4.1: Experimental end cap dimensions

It should be noted that the end caps were connected to the piezoelectric element by use of a special solder and flux purchased from the manufacturer. More specifically, the solder was used to connect the bottom of the end caps to the nickel electrodes that were fired on the top and bottom surface of the piezoelectric material. Although alternative solutions, such as various cyanoacrylates and epoxies, would also produce a strong mechanical bond, a solder joint has the advantage of providing a solid electrical connection as well. This would allow for the connection of the lead wires to the end caps instead of directly connecting them to the nickel electrodes on the piezo. This meant that the cap height could be lowered significantly as not nearly as much clearance would be necessary as it would be to accommodate a solder joint to the top and bottom of the electrodes. However, in order to attach a center tap wire for parallel operation, the height was increased somewhat in order to give some forgiveness

between the end cap and the piezo electrodes. Also, if the center tap wire should happen to disconnect during the experiment, there was enough room left to reattach the wire without having to disassemble the prototype or experimental setup. As a result, the resonance frequency of the device is higher than the resonances of typical industrial vibration sources. A prototype of the carriage spring energy harvester is shown in Figure 4-2. Figure 4-2 (a) shows the actual prototype that was used throughout the entire experimentation phase while Figure 4-2 (b) shows a Computer Aided Design (CAD) representation of the device that was used for the purposes of explaining to the manufacturer exactly where to drill for the center tap.



(a) Actual



(b) CAD

Figure 4-2: Carriage spring end caps assembly showing (a) actual assembly and (b) CAD representation

## 4.2 Experimental Setup

Designing the prototype was only one step in the experimentation process. A mounting bracket had to be constructed to hold the device and correctly align the mass, while a test bed had to be fabricated in order to accommodate the mounting bracket and the exciter. A detailed diagram of the mounting bracket, shaker, and sensors is shown in Figure 4-3. The experimentation process is described thoroughly in the following sections and a flowchart describing the procedure is outlined in Figure 4-4.

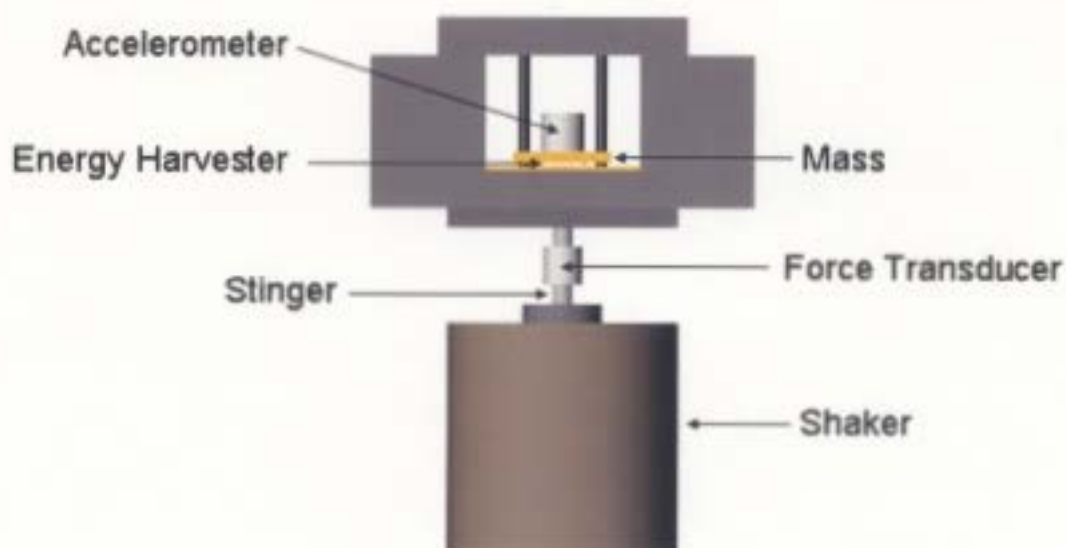


Figure 4-3: Detailed diagram of mounting bracket, shaker, and sensors

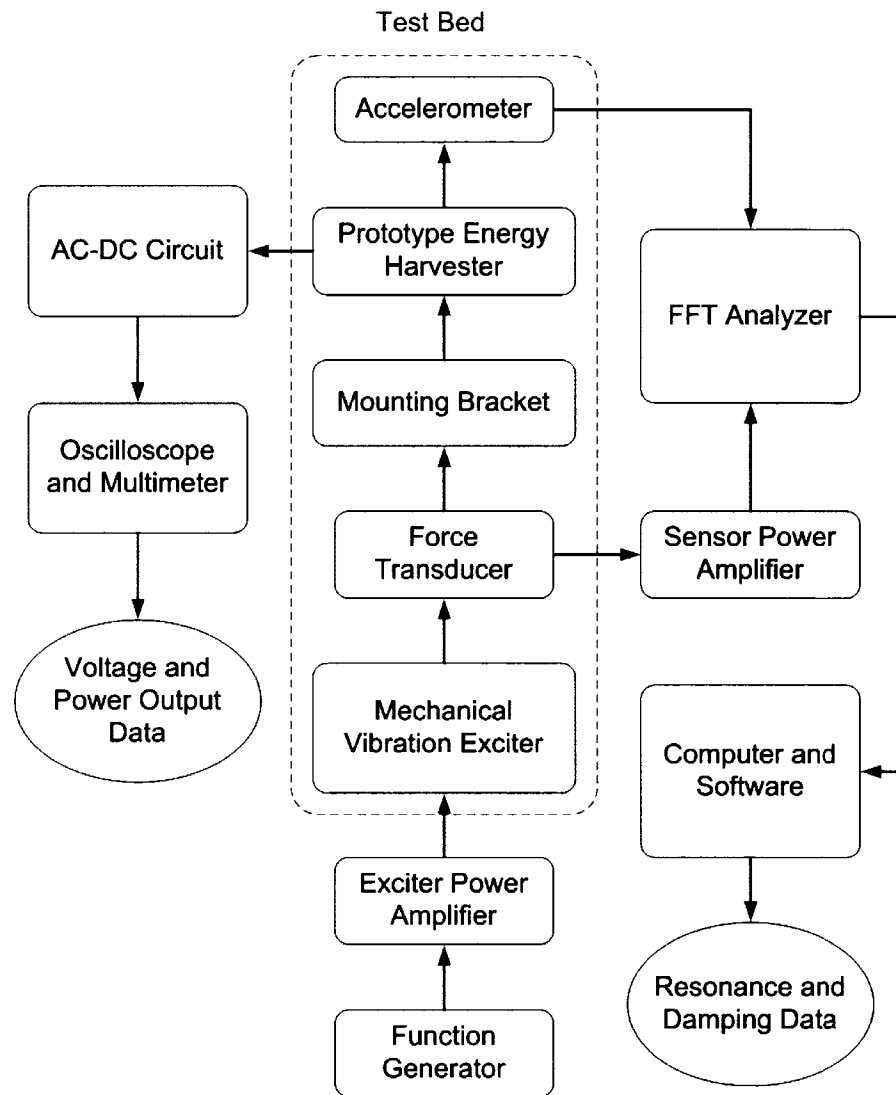


Figure 4-4: Experimental setup flowchart

### 4.2.1 Mechanical Setup

After constructing the prototype, a mounting bracket was constructed out of a Polyvinyl Chloride (PVC) material as shown in Figure 4-5. This mounting bracket was designed to hold the energy harvester as well as provide a means by which to control the direction of motion of the mass. To accomplish this, a 50g mass was cut out of copper. This copper mass then had two equally sized holes drilled on either side so that it could slide freely in only one direction along the two small plastic rods shown in Figure 4-5. Two 2.5cm tall plastic sleeves were then attached to the mass to slide with the mass along the plastic rods. These plastic sleeves, along with a small amount of grease, were used to prevent the mass from binding on the rods during experimentation. The mass was then glued using a strong cyanoacrylate glue to the top section of the top end cap, labeled as  $B_{cm}$  in Figure 4-1.



Figure 4-5: Carriage spring mounting bracket showing (a) actual assembly and (b) CAD representations

Next, the bottom end cap was glued to a copper mount, which was glued to the base of the mounting bracket. It should be noted that as an alternative to screws, glue was used wherever possible to connect the various sections of the mounting bracket together. This was done so that the accelerometers would not pick up the rattle of the screws during excitation and interfere with the experimental resonance frequency

analysis of the device. In fact, the entire mounting bracket is assembled with only two screws.



(a) Actual



(b) CAD

Figure 4-6: Steel test bed assembly showing (a) actual assembly and (b) CAD representation

In addition to the mass being constrained to only vertical motion, the mounting bracket also had to be constrained to purely vertical motion. To accomplish this, holes were drilled along the sides of the mounting bracket such that the bracket could move freely along the steel rods of the testbed shown in Figure 4-6. Figure 4-5 (a) and (b) are slightly different with respect to these holes. The original design called for two holes to be drilled down the entire distance from the top of the mounting bracket to the bottom of the mounting bracket, as shown in Figure 4-5 (b). However, drilling this proved to be more difficult than originally anticipated. Consequently, cutting a small section of PVC from each side of the bracket allowed the drill bit to not have to remove as much material, thus simplifying the fabrication process. The actual mounting bracket is shown in Figure 4-5 (a). Finally, a small threaded hole

was drilled in the bottom of the mounting bracket in order to connect the bracket to the exciter through a threaded steel stinger.

The test bed was constructed of heavy duty 1.27cm steel and placed on a rubber mat on a steel frame to reduce the unwanted vibration sources that perpetuate throughout the lab. The testbed was quite simple in design. It consisted of a simple frame with two steel rods used for the accommodation of the mounting bracket. The exciter was firmly screwed to the base of the test bed, and the test bed was securely fastened to the steel frame. Figure 4-6 shows a small bungee wrapped around the mounting bracket and test frame. The purpose of this is to try to reduce the weight of the mounting bracket on the exciter to reduce the interference of the mounting bracket's mass with the internal mass of the exciter. The bungee allows the mounting bracket to "hang freely" and is consistent with generally practiced resonance analysis techniques found in [36].

#### **4.2.2 Electrical Setup**

Figure 4-7 shows the electrical equipment used throughout the experimentation process. The equipment shown in the figure includes a function generator and a large power amplifier used to control the frequency and amplitude of the exciter vibration. The figure also shows a smaller power amplifier which is used to amplify the signal of the force transducer positioned between the stinger and the mounting bracket in Figure 4-5.

In addition, there are a few multimeters, cable buses, oscilloscopes, and other miscellaneous electronic equipment shown in the figure. However, the most utilized piece of equipment shown is the Fast Fourier Transform (FFT) analyzer located on the far right of Figure 4-7. This FFT analyzer is very useful in determining the resonance frequencies and damping ratios of various test specimens. Consequently, the use of this FFT analyzer will be discussed more thoroughly in the following section.



Figure 4-7: Various electrical equipment utilized during experimentation

## 4.3 Experimentation

### 4.3.1 Resonance Frequency Analysis

The procedure to determine the resonance frequencies and damping ratios of different energy harvesters is as follows. First, a small accelerometer was attached to the copper mass with generic poster putty, and a force transducer was screwed tightly between the threaded stinger and mounting bracket. A function generator was then connected to the exciter through a power amplifier. Both outputs of the accelerometer and force transducer were then connected to the FFT analyzer.

Next, the function generator was set to sweep a sinusoidal bandwidth of  $10 - 400\text{Hz}$  over a two-second timespan and the FFT analyzer was initialized with the same time scale. Once the function generator began sweeping the frequencies, the FFT analyzer recorded the accelerometer results and conducted a standard FFT transform to determine the frequency response of the system. The frequency response

of the above mentioned prototype with a 55g mass is shown in Figure 4-8 (a). A very distinct frequency peak of 154.5Hz can be seen in the graph.

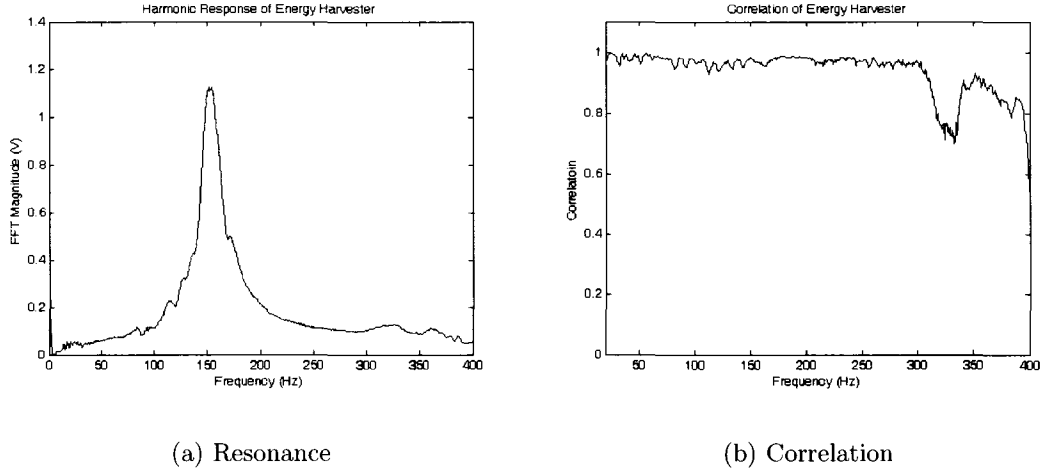


Figure 4-8: Energy harvester (a) frequency response and (b) correlation

In order to calculate the damping ratio, the amplitude,  $A_p$ , of the peak was observed and the frequencies at which an amplitude of  $\frac{A_p}{\sqrt{2}}$  occurred on either side of the peak were reordered. These two frequencies were used in the Equation 4.1 to determine the damping ratio. The damping ratio for this particular prototype with a 55g mass was calculated to be 4.91%. The reason for this high damping ratio value is most likely due to frictional forces between mass and the plastic rods. A damping ratio of this magnitude has the disadvantage of requiring a larger input acceleration in order to generate power; however, the energy harvester does have the advantage of an increased operating bandwidth.

$$\zeta = \frac{f_2 - f_1}{f_1 + f_2} \quad (4.1)$$

where

$$\zeta = \text{damping ratio [-]}$$

$$f_1 = \frac{A_p}{\sqrt{2}} \text{ frequency value to the left of } A_p \text{ [Hz]}$$

$$f_2 = \frac{A_p}{\sqrt{2}} \text{ frequency value to the right of } A_p \text{ [Hz]}$$

The purpose of the force transducer was to measure the exact input force into the system. This allowed the FFT analyzer to combine the accelerometer output with the force transducer output to produce a correlation factor. This correlation factor basically explains how much of the observed frequency response is explained by the input vibration of the exciter. As can be seen in Figure 4-8 (b), the correlation is extremely close to one (100%) over most of the frequency range. However, there appears to be a large dip in correlation after 300 Hz. This is most likely due to various unwanted resonances within the mounting bracket itself, such as screws and various other connection points. Regardless, the graph shows a very high correlation over the frequency span of interest.

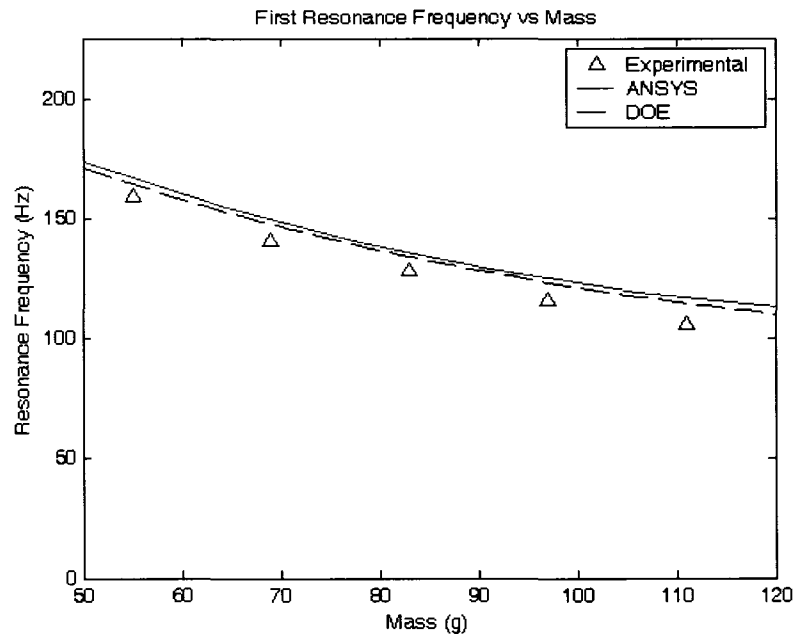
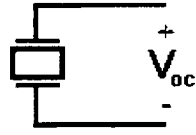


Figure 4-9: Energy harvester resonances vs. mass

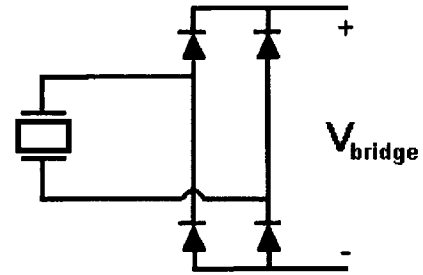
To determine the different resonance frequencies of the prototype with different masses, the procedure described above was carried out for a 55g, 69g, 83g, 97g, and 111g mass. The original 50g mass was increased by incrementally securing smaller 14g masses on top of the 50g mass with high grade double-sided tape. The mass is actually recorded as 5g heavier in order to account for the additional mass of the accelerometer. Figure 4-9 shows the experimental results along with the Ansys and DOE model results. The experimental results seem to be in good agreement with the theoretical results; however, they seem consistently lower than the models. This is most likely due to the fact that the piezoelectric tolerances given by the manufacturer are only accurate to within  $\pm 10\%$ . Also, in order to attach the smaller 14g masses to the 50g mass, a small amount of pressure had to be applied to get the mass to stick properly. This, ultimately, may have compressed the height of the end caps, thus lowering the resonance frequencies. The same argument can be said for attaching the accelerometer to the mass. This is the main reason why the results for the 50g mass in Figure 4-8 (a) do not exactly match the results in Figure 4-9 as the results for Figure 4-8 (a) were recorded after the resonance frequency vs. mass experiment had been completed. Nevertheless, the experimental values were all within 2.35% of the modeled values, thus providing very promising validating of the mechanical models.

### 4.3.2 Electrical Analysis

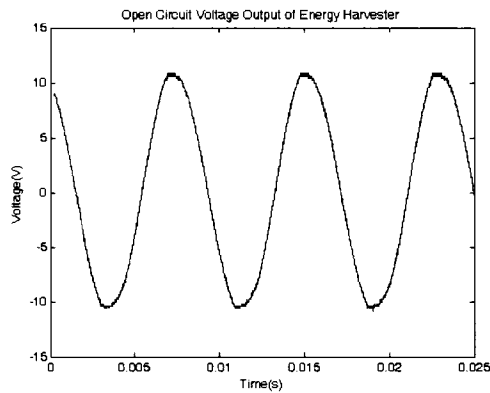
Figure 4-13 shows a sample voltage output of the prototype energy harvester with a 55g mass excited at its resonance frequency of 154.5Hz with a base acceleration of 1.4g's. The energy harvester achieved an AC open circuit output voltage of approximately 10.8V. Figure 4-10 (c) shows this output and Figure 4-10 (a) shows the simple circuit schematic used to acquire this data. A bridge rectifier was added to convert the AC voltage to DC voltage and is shown in Figure 4-10 (b). The output of the bridge, in Figure 4-10 (d), shows that all negative voltages of the sinusoid have been converted into positive voltages.



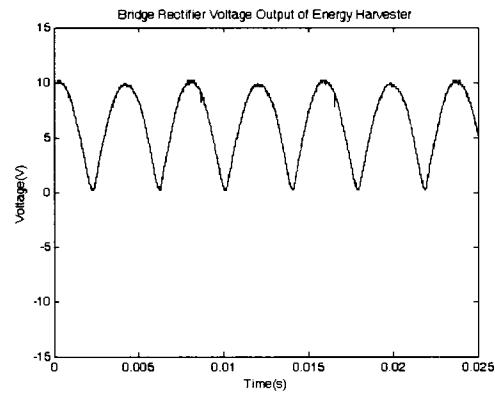
(a)  $V_{oc}$  Circuit



(b)  $V_{bridge}$  Circuit



(c)  $V_{oc}$



(d)  $V_{bridge}$

Figure 4-10: Energy harvester DC (a)  $V_{oc}$  circuit, (b)  $V_{bridge}$  circuit, (c)  $V_{oc}$  output voltage, and (d)  $V_{bridge}$  output voltage

However, in order to achieve a proper DC signal, a capacitor must be added, as shown in Figure 4-11 (a), to smooth out the signal. Notice that this circuit's corresponding signal, shown in Figure 4-11 (c), now has a voltage magnitude of approximately  $9.5V$ , which is approximately  $1.3V$  less than the maximum voltage observed in Figure 4-10 (c). This is quite consistent with what is expected to occur after a sinusoidal signal passes through a bridge. An “ideal” diode has a voltage drop of approximately  $0.7V$ . Due to the fact that two diodes are always experiencing their *on*-state at any given time during the AC-to-DC transformation, a voltage drop of

1.4V ( $0.7V + 0.7V$ ) is expected. The 0.1V discrepancy between the theoretical and experimental values is due to the fact that in actual practice a diode is rarely ever “ideal”.

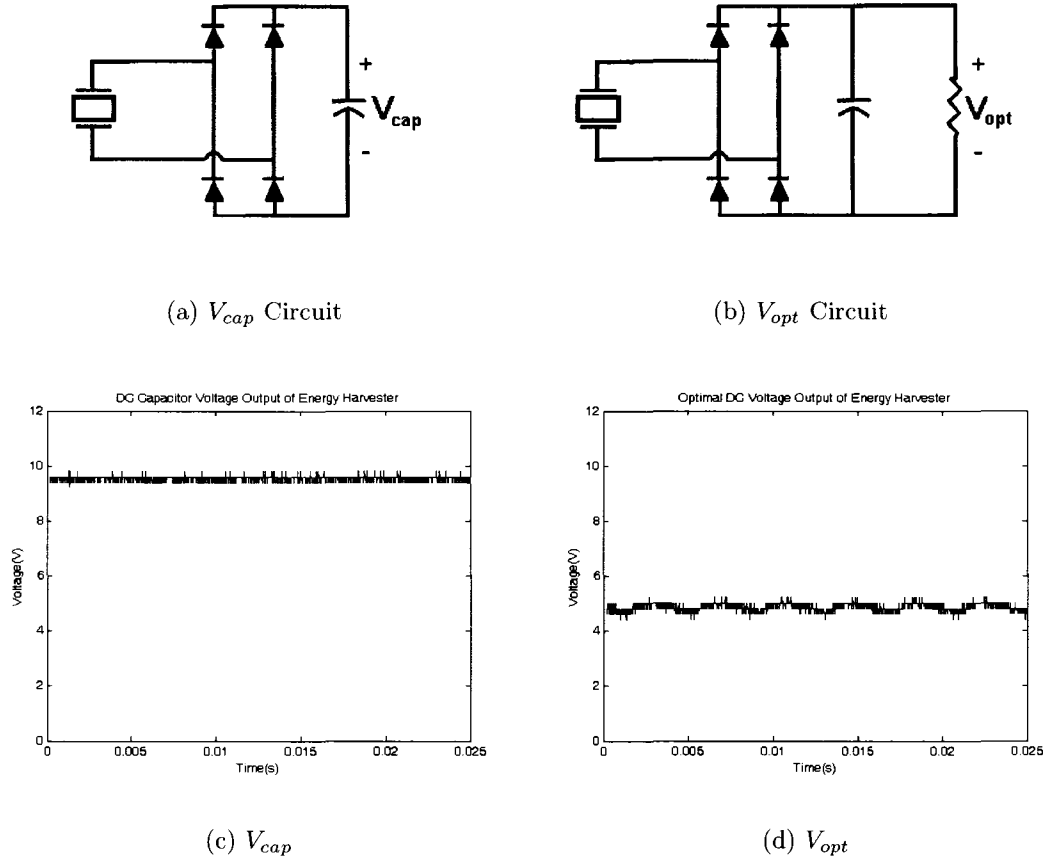


Figure 4-11: Energy harvester DC (a)  $V_{cap}$  circuit, (b)  $V_{opt}$  circuit, (c)  $V_{cap}$  output voltage, and (d)  $V_{opt}$  output voltage

Figure 4-11 (b) shows the schematic used in order to obtain maximum power transfer to a load resistor. The optimal DC output voltage,  $V_{opt}$ , necessary to obtain maximum power transfer is always one half of the open circuit voltage observed across the DC terminals,  $V_{cap}$ . As a result, adjusting  $V_{opt} = \frac{1}{2}V_{cap}$  should produce the maximum DC power. Figure 4-11 (d) shows a DC voltage of approximately 4.8V, which is the optimum voltage needed to obtain maximum power transfer. The

maximum DC power is obtained via the standard electrical power equation shown in Equation 4.2.

$$P = \frac{V^2}{R} \quad (4.2)$$

where

- $P$  = power [W]
- $V$  = voltage [V]
- $R$  = resistance [ $\Omega$ ]

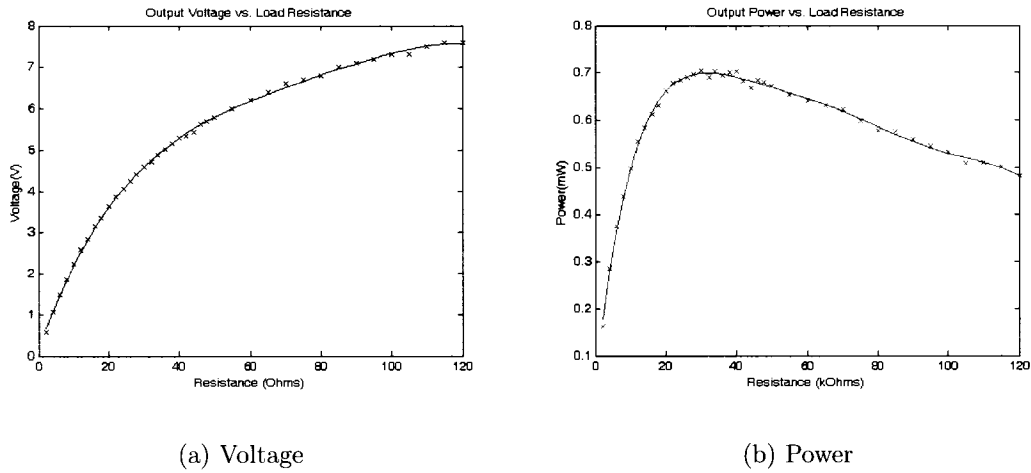


Figure 4-12: Energy harvester DC (a) voltage output and (b) power output

Figure 4-12 shows how the resistance value changes the voltage and power output obtainable from the device. Figure 4-12 (a) shows the observed output voltage while 4-12 (b) shows the output power. For this experiment it should be noted that with the same acceleration and frequency input values as those used previously, the output across the bridge increased slightly from 9.5V to 10.1V due to slight resistance fluctuations generated by the self-heating of the piezoelectric element. Consequently, the optimal voltage shown in Figure 4-12 (a) is approximately 5V, which is nearly

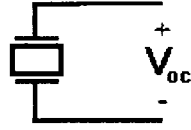
one half of the DC open circuit voltage as expected. The optimal resistance shown in 4-12 (b) is  $36.1k\Omega$ , which produces a maximum power of  $0.71mW$ . It is worth noting that although there is high penalty for having a resistance lower than optimal, there is only a slight penalty for having a resistance that is more than optimal. This means that any resistive circuit connected to a piezoelectric energy harvester should be designed to have a resistance equal to or above the optimal resistance. Additionally, any other type of circuit, such as a capacitive battery charging circuit, should always be designed to charge at one half the open circuit voltage across the DC terminals or slightly above.

### 4.3.3 Maximum Mechanical-to-Electrical Conversion

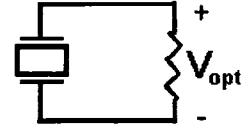
To determine the maximum average power that could be harvested from the device, the prototype was excited at its resonance frequency. The manufacturer suggests that the maximum strain be kept under  $500\mu\epsilon$  which has been shown in previous Ansys models to be equivalent to an open circuit voltage of approximately  $47V$ . In order to ensure that the piezo did not break,  $4.9g$ 's was a sufficient acceleration to produce  $40V$  across the energy harvester terminals and was deemed adequate for the tests.

Both AC and DC experiments were conducted to investigate how the losses from the AC-DC circuitry affected the output power and efficiency. Figure 4-13 (a) and Figure 4-13 (b) show the simple AC circuit setups that were used to produce Figure 4-13 (c) and Figure 4-13 (d) respectively. Notice that for maximum AC power transfer, the voltage across the resistor is one half the open circuit voltage across the AC terminals. This is shown in Figure 4-13 (d). The average AC and DC power details are shown in Table 4.2. It should be noted that the AC power was calculated using the average power Equation 1.14.

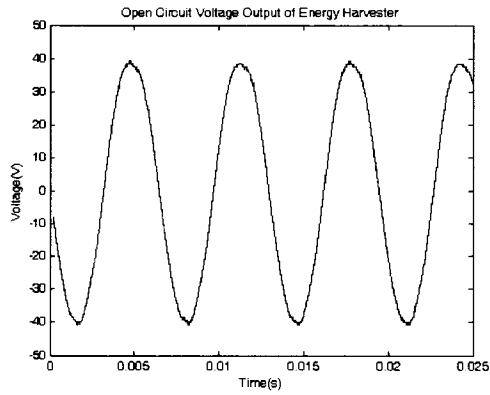
By observing the maximum AC and DC power obtainable from the PZT piezo purchased from Piezo Systems Inc., it is quite obvious that a large amount of power is lost in the AC-DC conversion process. In fact, for this experiment, almost 29% of the



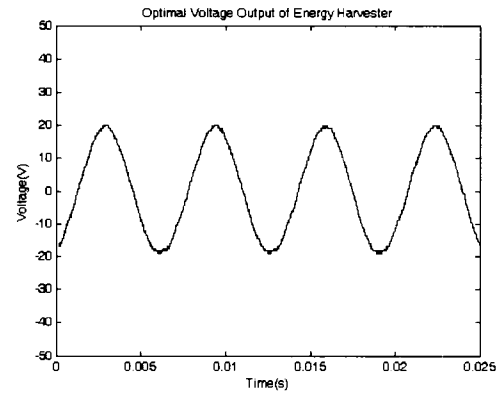
(a)  $V_{oc}$  Circuit



(b)  $V_{opt}$  Circuit



(c)  $V_{oc}$



(d)  $V_{opt}$

Figure 4-13: Energy harvester AC (a)  $V_{oc}$  circuit, (b)  $V_{opt}$  circuit, (c)  $V_{oc}$  output voltage, and (d)  $V_{opt}$  output voltage

AC power was lost through the rectification circuitry. This is the main reason why AC-DC rectification is still the main hurdle in low-power energy harvesting through vibration. Fortunately, a lot of work has gone into this area recently. Attempts to produce switch-based as apposed to diode-based rectification, such as Siebert's work in [37], looks promising for the future.

Description	Symbol	Units	DC Value	AC Value
Input Acceleration	$\vec{a}$	g's	4.9	4.9
Input Frequency	$f_{in}$	Hz	154.5	154.5
Damping Ratio	$\zeta$	%	4.91	4.91
Open Circuit Voltage	$V_{oc}$	V	40.6	40.0
Optimal Load Voltage	$V_{opt}$	V	19.75	20.0
Optimal Resistance	$R_{opt}$	k $\Omega$	24.7	9.0
Maximum Power	$P_{max}$	mW	15.79	22.22

Table 4.2: Experimental maximum power data

#### 4.3.4 Efficiency Investigation

In order to observe the behavior of the prototype energy harvester over a variety of different base excitation levels, a small experiment was set up. The prototype was fitted with three different masses and the resonance frequencies and damping ratios were recorded. The prototypes were then excited and the resistance adjusted for each in order to obtain *maximum* power transfer. Once the optimal voltage and resistance were obtained, the maximum power could be obtained via Equation 4.2. The data for a prototype loaded with a 55g, 83g, and 111g mass is shown in Table 4.3.

Description	Symbol	Units	55g	83g	111g
Resonance Frequency	$f_{res}$	Hz	158.78	127.96	105.72
Mechanical Damping Ratio	$\zeta_m$	%	4.91	7.29	9.78

Table 4.3: Data pertaining to prototypes loaded with three different masses

The table shows that the resonance frequency decreases with increasing mass and the damping ratio increases with increasing mass. To determine the maximum theoretical power that can be achieved for a 100% efficient energy harvester, Equation 1.4 is used. This equation only holds when the frequency of the base driving force exactly matches the resonance frequency of the the energy harvester. It should be noted that in order to determine the *maximum* achievable power, the total damping ratio,  $\zeta_T$ , was set to equal  $2\zeta_m$ . This relation holds only for maximum power for the reasons discussed in Section 1.2.1. To reiterate, the maximum power transfer occurs when  $\zeta_e = \zeta_m$ . Because we know  $\zeta_m$  through the FFT frequency analysis, we also know that  $\zeta_e$  will have the same value when maximum power output is occurring. Due

to the fact that the optimal resistance, which is directly proportional to  $\zeta_e$ , is always chosen for this series of tests, we can assume that the relation  $\zeta_T = 2\zeta_m$  will hold.

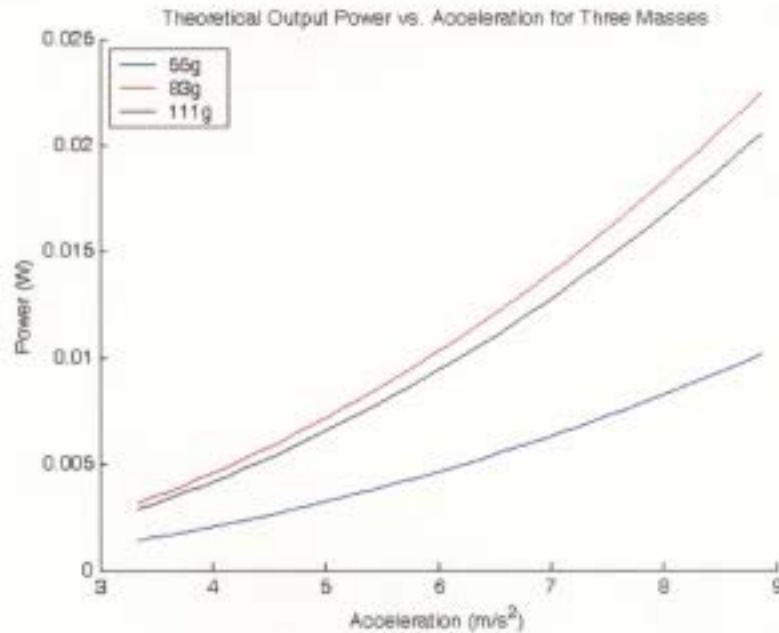


Figure 4-14: Theoretical power vs. base acceleration

Figure 4-14 shows the theoretical power that can be produced for the three masses at their corresponding resonance frequencies. One may expect that a heavier mass would be able to produce more power, and with all other factors being equal, it does. However, in this case, the changing mass affects the damping ratio and resonance frequencies, which have a major impact on the power that can be produced. This is the reason why measuring efficiency in this way can be quite misleading. Assuming a prototype with a decreased damping ratio were created by removing the plastic rods that are used to align the mass, the theoretical power would be increased dramatically. This is why it is important to carefully state that the maximum power shown in Figure 4-14 is the maximum obtainable power *at that particular damping ratio*. Nevertheless, Figure 4-14 does provide a good benchmark to gauge how well the real energy harvester is performing.

Figure 4-15 shows the experimental AC and DC maximum power distributions

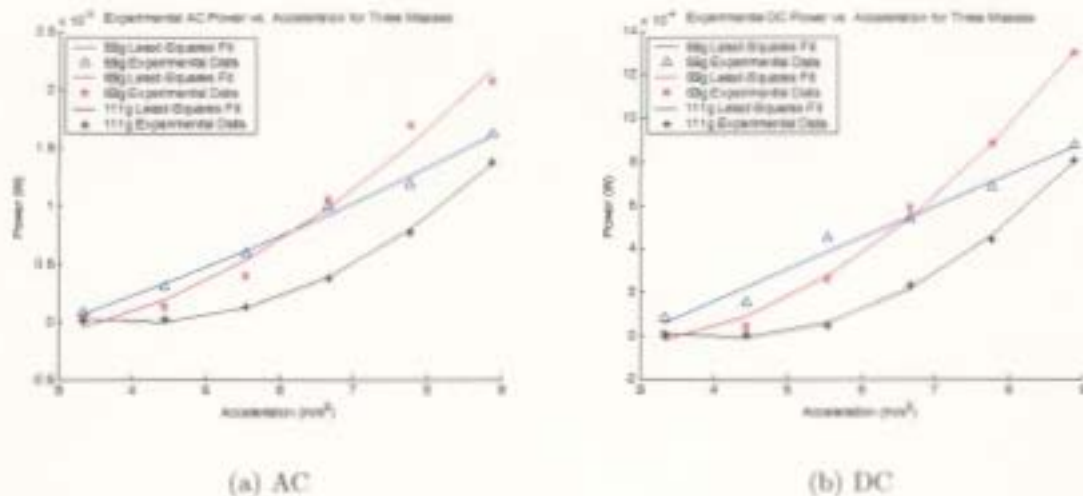


Figure 4-15: Maximum power output vs. base acceleration for an (a) AC circuit and (b) DC circuit

over a changing input excitation. Although the graphs do not appear to directly match the graph in Figure 4-14, if one could imagine extending the lines in Figure 4-15, the graphs would align quite well. It can also be seen that the lines in the experimental graph do cross each other, whereas the line in the theoretical graph do not. This is due to the fact that the theoretical model does not take the mechanical limits of a true mechanical system into account. In other words, although the lighter energy harvester produces less power, it can start producing more power under small excitations than the heavier, highly-damped energy harvesters. As the excitation level is increased and the critical damping value is surpassed, the experimental and theoretical graphs will line up much better.

Mass [g]	$\zeta_T$ [%]	$\eta_{AC}$ [%]	$\eta_{DC}$ [%]
55	9.82	16.1	9.7
83	14.58	9.65	5.8
111	19.56	6.6	3.9

Table 4.4: Efficiencies of three different prototypes

Figure 4-16 shows the efficiencies for the three different energy harvesters. It would appear that the lighter, less-damped energy harvesters are the most efficient. This

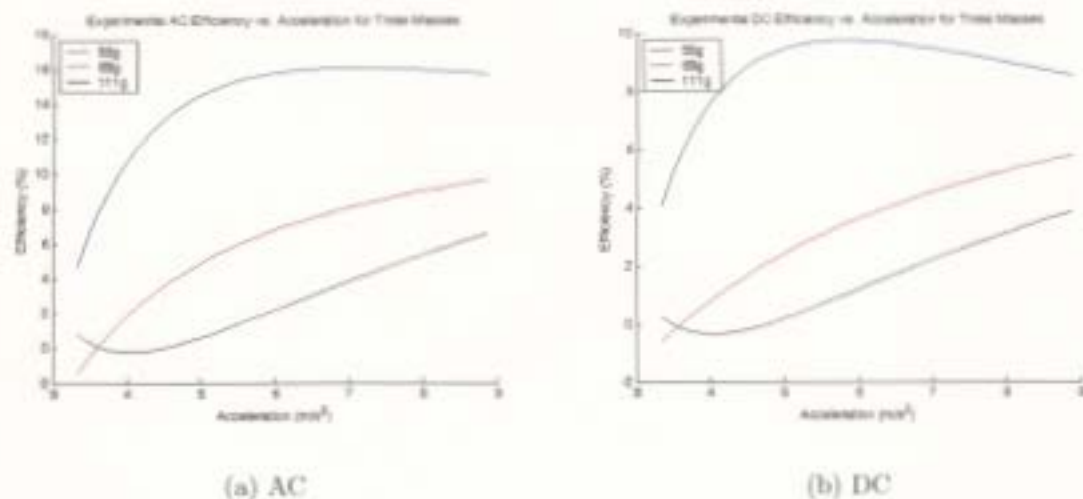


Figure 4-16: Energy harvester efficiency vs. base acceleration for an (a) AC circuit and (b) DC circuit

makes intuitive sense as an energy harvester with less damping has a much steeper modal peak that will produce more power. Therefore, it is reasonable to assume that efficiency can be increased by lowering the damping ratio at a cost of having a smaller bandwidth. The maximum efficiencies,  $\eta_{AC}$  and  $\eta_{DC}$ , for the different prototypes are outlined in Table 4.4. The efficiency for the two devices are quite low. This value could be increased by using better piezoelectric materials, eliminating the center shim, and eliminating the mass sliding rods. The DC efficiency could be brought closer to the AC efficiency by adding additional electronic components, such as those discussed by Deng in [27], or by investigating ways to remove the power-hungry bridge rectifier, as proposed in Appendix C.

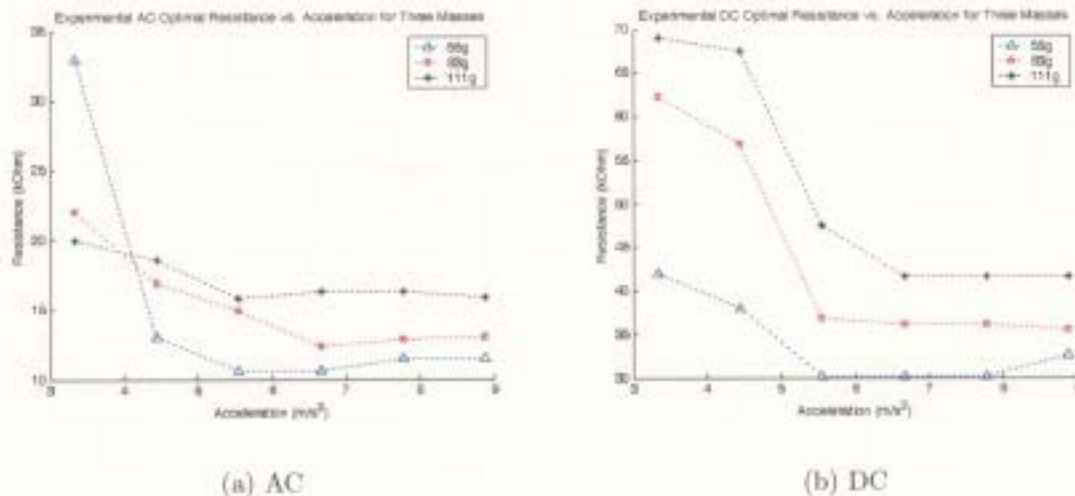


Figure 4-17: Optimal resistance vs. base acceleration for an (a) AC circuit and (b) DC circuit

Figure 4-17 shows how the optimal resonance frequency for each prototype is affected by the input excitation. It would appear that at low excitations, when the device is attempting to overcome its critical mechanical damping value, the optimal resistance is very high. This leads to very low power initially. However, it would appear that after the system has overcome this hurdle, the optimal resistance begins to stabilize to a constant value and the power begins to increase dramatically. This phenomena is very fortunate as it leads to circuitry design that can produce optimal power over an almost unlimited range of excitation amplitudes.

# Chapter 5

## Conclusions and Future Work

### 5.1 Energy Harvester Design Conclusions

Through the experimentation conducted, several phenomena of interest can be seen which dictate how one should design an energy harvester based on certain criteria. If the excitation levels are extremely high, and the base frequency constantly changing, one should design an energy harvester to have the following features:

1. The energy harvester resonance should match the base frequency as closely as possible. Also, given the same input acceleration, designing for the lowest frequency in the spectrum will produce the most power
2. The energy harvester should have mechanical stops to prevent the device from breaking.
3. A large mass will ensure that large amounts of power are produced.
4. The damping ratio should be large to accommodate the changing base frequency (Consider a cymbal or carriage spring design).
5. For capacitive battery charging, always design circuitry such that the battery or capacitor is always charging at one half the DC open circuit voltage of the

piezo. For resistive loads, designing the circuitry at or slightly above the optimal resistance will ensure that the load voltage is one half the DC open circuit voltage and therefore transferring maximum power.

6. Increased bandwidth, not efficiency is the primary goal.

If the excitation level is low and the base frequency is relatively constant, one should design this type of energy harvester to have the following features:

1. The energy harvester resonance should match the lowest-frequency highest-amplitude frequency in the base excitation spectrum as closely as possible
2. A small mass will ensure that some amount of power can be produced even at low excitation levels as the critical damping will be easier to overcome.
3. The damping ratio should be small in order to obtain as much power as possible from the given input vibrations (Consider a cantilever beam or carriage spring design).
4. For capacitive battery charging, always design circuitry such that the battery or capacitor is always charging at one half the DC open circuit voltage of the piezo. For resistive loads, designing the circuitry above the optimal resistance will ensure that a greater amount of power can be obtained during very low excitations.
5. Efficiency is the primary goal here. not increased bandwidth.

Unfortunately, the most common situation that arises in structural health monitoring is a very small input vibration occurring at a fluctuating frequency. The best approach to deal with this situation would be to follow the guidelines of the low-excitation, constant-frequency spectrum approach. However, the damping ratio should be adjusted in order to increase the bandwidth to an application-specific feasible amount without compromising the ability of the harvester to produce significant

amounts of power. An alternative to increasing the damping ratio would be to actively adjust the resonance frequency of the device to accommodate a changing frequency spectrum. However, doing this requires adjusting physical properties of the device, which ultimately requires large amounts of electrical power to move motors, tighten shape memory alloy wire, alter Magneto-Rheological (MR) fluid, etc. The amounts of power required to do this usually far exceed the power actually being produced by the device.

No matter what excitation environments exist, energy harvester design has the potential to be quite difficult. A designer must carefully study the design criteria and prioritize which features are most important given the vibration levels and application. Ultimately, a good understanding of how piezoelectric energy harvesters work coupled with a great amount of planning and common sense should lead to a good design.

## 5.2 Future Investigation

This thesis began by taking a very broad look at energy harvester design for the purposes of energy harvesting for structural health monitoring systems. Although the work conducted here drew meaningful conclusions and recommendations on how to design an energy harvester for different environments, it did not specifically focus on how to design for a real structural health monitoring situation. The experimental work showed that effective power harvesters could be used given very high acceleration environments found mostly on high powered industrial equipment. However, in order to design an energy harvester that runs on the low frequency ( $< 50\text{Hz}$ ), low acceleration ( $< 1g$ ) levels found on most civil structures, quite a different strategy is needed. As a result, the following should be further investigated by anyone who has a great deal of interest in this subject.

- Calculate the total possible power that is harvestable from different structural environments in order to determine if power harvesting is feasible given common energy harvesting techniques and materials. Some environments of interest could include ship hulls, FPSOs, aircraft wings, spacecraft, and railways.
- Determine both the mechanical and electrical tradeoffs between a carriage spring design and a cantilever beam design at low frequency levels. For low frequency environments, a cymbal would be quite unfeasible.
- Scalability is a major area for future research. Scaling down the energy harvesters discussed in this thesis and modeling them in Ansys would be a very interesting endeavour. As discussed in Section 5.1, the best solution would have low damping, low mass, and small size. Also, the piezo material should be as small as possible to produce a significant amount of voltage. Bringing these values to their physical limits would help to investigate whether or not it is feasible to overcome the inertial damping present in these energy harvesters to produce any significant power.

- Investigate new piezoelectric materials that have higher mechanical to electrical conversion efficiencies, such as PZN-PT, in order to design the most efficient energy harvester possible.
- Investigate possible solutions to automatically adjust the resonance frequency of the device to match the dynamically changing vibration frequency of the input vibration. Also, investigation into cascading generators to increase bandwidth, such as those proposed by Deng in [27], would prove worthwhile.
- Investigate ways to remove the bridge rectifier circuitry, which is the primary cause of power loss during AC-DC power conversion. In fact, for generating very low amounts of power from small vibration sources, the diode loss hurdle (1.4V) *must* be overcome in order to generate any power at all. This is, in the author's opinion, the most important area for future research for vibration energy harvesting from civil structures. A potential solution to this problem is proposed by the author in Appendix C.

Great strides will be made in mechanical-to-electrical power harvesting only when these items are given the necessary attention by the scientific community. Wireless solutions, such as Zigbee wireless sensor networks, continue to make large strides in power efficiency; however, the physical limits imposed by today's current batteries are not equipped to handle the large scale wireless sensor networks envisioned by industrial engineers and companies. Consequently, it is believed by the author that these technologies will serve only on a limited basis until realistic energy harvesting techniques are discovered. The *ONLY* way to achieve this is through the conglomeration of knowledge pertaining to this subject across three major scientific disciplines, namely mechanical engineering, electrical engineering, and material science.

# Appendix A

## Ansys Carriage Spring Code

```
/title, Static Analysis of Carriage Energy Harvester
/filename,bw3
/nopr
/com
/Prep7
/RGB,INDEX, 100, 100, 100, 0
/RGB,INDEX, 80, 80, 80, 13
/RGB,INDEX, 60, 60, 60, 14
/RGB,INDEX, 0, 0, 0, 15

!-----
! User Variables
!-----

m = 275e-3
h = 1e-3
a = 2.5e-3
b = 10.9e-3
c = 2.5e-3
w = 6.4e-3
```

```
tpiez = .13e-3
tshim = .12e-3
tcap = .254e-3
massDens = 1700000
disp = -.22e-3
```

```
! Calculated Variables
```

```
!w = 3.14*b/2
hm = m/(a*w*massDens)
tp = tpiez
ts = tshim/2
tt = ts+tp
t = tcap
```

```
!-----
```

```
! Draw Device
```

```
!-----
```

```
local,11 ! Coord. system for lower layer: polar axis +Y
local,12,,,,,180 ! Coord. system for upper layer: polar axis -Y
csys,11 ! Activate coord. system 11
```

```
!-----Draw Keypoints for cap
```

```
k,1,0,h $ k,2,a,h $ k,3,a+b,0 $ k,4,a+b+c,0 $ k,5,0,h+t
k,6,a,h+t $ k,7,a+b,0+t $ k,8,a+b+c,0+t
```

```
!-----Draw Lines for cap
```

```
l,1,2 $ l,2,3 $ l,3,4 $ l,5,6 $ l,6,7 $ l,7,8 $ l,1,5 $ l,4,8
```

```

!-----Draw Cap Area
al,all ! draw areas by lines
AGEN,2,ALL,,,tt,,,1 ! make room for piezo
arsym,y,all ! reflect area

!-----Draw Keypoints for Mass and Piezo
k,17,0,h+t+hm+tt $ k,18,a,h+t+hm+tt $ k,19,0,tt $ k,20,0,-tt
k,21,0,ts $ k,22,0,-ts $ k,23,a+b+c,ts $ k,24,a+b+c,-ts

!-----Draw Lines for Mass and Piezo
1,5,17 $ 1,6,18 $ 1,17,18 $ 1,19,21 $ 1,21,22 $ 1,22,20
1,4,23 $ 1,23,24 $ 1,24,12 $ 1,19,3 $ 1,20,11 $ 1,21,23 $ 1,22,24

!-----Draw Mass and Piezo Area
al,4,17,18,19 ! draw areas by lines for mass
al,20,26,28,3,23 ! draw top piezo
al,22,29,27,11,25 ! draw bottom piezo
al,21,28,29,24 ! draw shim
aglu,all ! glue areas

!-----
! Define Material Constants
!-----
EMUNIT,EPZRO,8.85E-12 ! free space

!-----Defin Material
et,1,plane223,1001 ! symmetric element
et,2,plane223,1001 ! symmetric element (for mass check)

```

```

!-----Defin Material Properties for cymbal and mass
mp,ex,1,130e9      ! Young's modulus for material ref. no. 1 (Brass Cap/Shim)
mp,ey,1,130e9
mp,dens,1,8400    ! density for material ref. no. 1 (Brass Cap/Shim)
mp,prxy,1,0.33 ! Poisson's ratio for material ref. no. 1 (Brass Cap/Shim)
MP,PERX,1,5 ! Low permittivity for center shim
MP,PERY,1,5
MP,PERZ,1,5

mp,ex,2,2e11      ! Young's modulus for material ref. no. 2 (Steel Mass)
mp,dens,2,massDens ! density for no. 2 (Steel Mass) - Exaggerated for display
mp,prxy,2,0.3 ! Poisson's ratio for material ref. no. 2 (Steel Mass)
MP,PERX,2,0
MP,PERY,2,0
MP,PERZ,2,0

!mp,ex,3,62e9 ! Young's modulus for material ref. no. 3 (Piezo)
!mp,dens,3,7800 ! density for material ref. no. 3 (Piezo)
!mp,prxy,3,0.3 ! Poisson's ratio for material ref. no. 3 (Piezo)

tb,anel,3 ! Stress matrix for ref. no. 3 (Piezo)
TBDATA,1,1.4357E+11,1.0108E+11,9.5678E+10
TBDATA,7,1.3541E+11,1.0108E+11
TBDATA,12,1.4357E+11
TBDATA,16,2.2989E+10
TBDATA,19,2.2989E+10
TBDATA,21,2.3946E+10

```

```
tb,piez,3 ! Piezoelectric matrix for ref. no. 3 (Piezo)
TBDATA,2,-10.8559
TBDATA,5,23.3268
TBDATA,8,-10.8559
TBDATA,10,17.0345
TBDATA,15,17.0345
MP,PERX,3,1704
MP,PERY,3,1302
MP,PERZ,3,1704
```

```
!-----
! Meshing
!-----
type,1
```

```
!-----Mesh Caps
lsel,all $ lesize,all,1e-4,,1 $ MAT,1 $ amesh,1 $ amesh,2
```

```
!-----Mesh Shim
lsel,all $ lesize,all,.5e-4,,1 $ MAT,1 $ amesh,6
```

```
!-----Mesh Piezo
lsel,all $ lesize,all,.4e-4,,1 $ MAT,3
esys,11 $ amesh,4 $ esys,12 $ amesh,5
```

```
!-----Mesh Mass
type,2
```

```

lssel,all
lesize,all,1700e-4,,1
MAT,2
amesh,3

!-----Define Nodes of Intrest
nMass = NODE(0,h+t+tt+hm,0)
nBotShim = NODE(0,-ts,0)
nTopShim = NODE(0,ts,0)
nBotPiez = NODE(0,-tt,0)
nTopPiez = NODE(0,tt,0)
nBotPiezEnd = NODE(a+b+c,tt,0)

nelec = 100 ! Number of electrodes on top surface
*dim,ntop,array,nelec
l1 = 0 ! Initialize electrode locations
!l2 = (b+c)/nelec
l2 = (a+b+c)/nelec
*do,i,1,nelec ! Define electrodes on top surface
nset,s,loc,y,0
!nset,r,loc,x,c+l1,c+l2
nset,r,loc,x,l1,l2
cp,i,volt,all
*get,ntop(i),node,0,num,min ! Get master node on top electrode
l1 = l2 + ts/10 ! Update electrode location
!l2 = l2 + (b+c)/nelec
l2 = l2 + (a+b+c)/nelec
*enddo

```

```

!-----
! Modal Analysis
!-----

!-----Find Solution
!/solu
!dl,7,,symm $ dl,16,,symm $ dl,17,,symm
!dl,20,,symm $ dl,21,,symm $ dl,22,,symm
!nsel,s,loc,y,-(h+t+tt) ! select bottom of device
!d,all,all,0
!nsel,all
!antype,modal ! modal analysis
!modopt,lanb,2 ! number of modes to extract
!mxpand,2 ! number of modes to expand
!solve ! solve
!fini

!-----Display Results
!/post1
!set,list ! show results
!set,first ! select first set
!pldisp,1 ! display deformed shape

!-----
! Static Analysis
!-----

/solu

```

```

dl,7,,symm $ dl,16,,symm $ dl,17,,symm
dl,20,,symm $ dl,21,,symm $ dl,22,,symm
antype,static ! transient analysis
acel,,9.8 ! apply gravity
nsel,s,loc,y,-(h+t+tt) ! select bottom of device
d,all,uy,0 ! constrain uy
nsel,all ! select all
nsel,s,loc,y,-tt          ! Define bottom electrode
d,all,volt,0             ! Ground bottom electrode
nsel,all
nsel,s,loc,y,tt          ! Define top electrode
d,all,volt,0             ! Ground top electrode
nsel,all

! apply load if necessary
d,nMass,uy,disp
!f,nMass,Fy,-mass*9.8
solve
finish

!-----Display Results
/POST26
ansol,2,nBotPiez,epel,x,botStrain
ansol,3,nTopPiez,epel,x,topStrain
NSOL,4,nMass,U,Y, UY_3
/com, - Spring Constant = %-m*9.81/uy(nMass)% N/m
/com, - Deflection ratio = %-ux(nBotPiezEnd)/uy(nMass)*100%

```

```
ntot = 0
*do,i,1,nelec
/com, - Electrode %i% Voltage = %volt(ntop(i))%
ntot = volt(ntop(i)) + ntot
*enddo
/com, - Electrode Average Voltage = %ntot/nelec% (Volt)
```

# Appendix B

## DOE Diagnostic Analysis

In order to determine if the model is actually statistically valid, a number of confidence interval criteria must be met. The testing for this type of significance is normally carried out graphically by the use of normal probability and residual-based diagnostic plots.

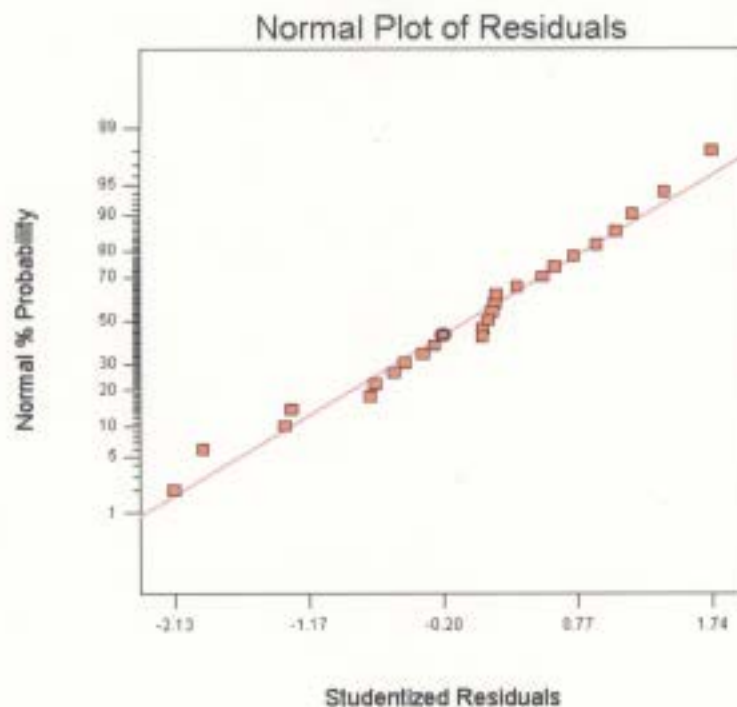


Figure B.1: Normal probability plot

Figure B.1 is a normal probability plot of the model. The normal percent probability values of the data are represented by the square boxes, while a standard normal probability graph is represented by the diagonal line. In essence, this plot represents how well the response follows a normal distribution. It is quite obvious that the response is quite "normal".

Figure B.2 shows the residuals vs. predicted plot. This plot shows how the residuals differ from the predicted response and is a measure of how well the model predicts. Ideally, one would like to see these values as close to zero as possible. However, it is common practice to be satisfied with the results as long as the residuals fall within the -3 and +3 as shown by the red lines on the graph.

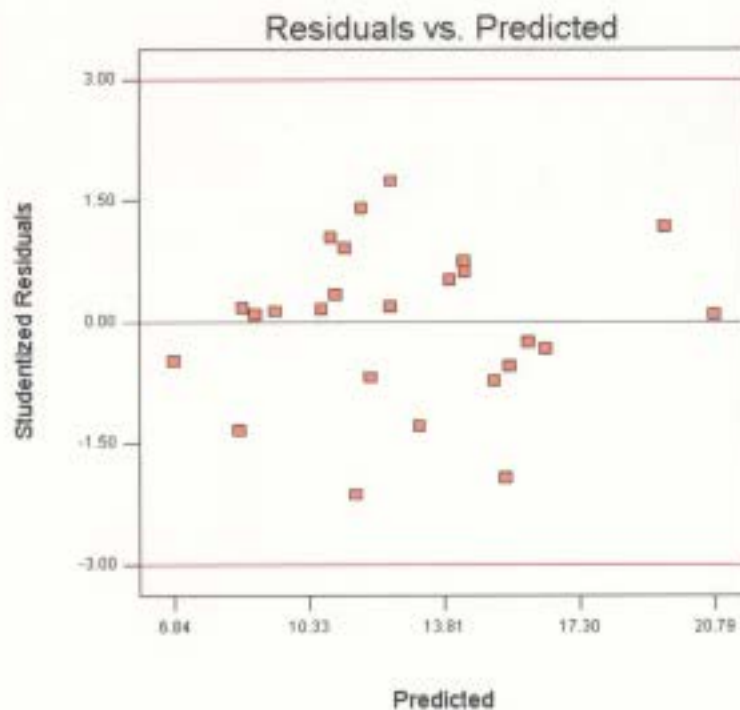


Figure B.2: Residuals vs. predicted

In addition, the plot of residuals vs. run, shown in Figure B.3, are not funnel shaped, and it can therefore be assumed that the process being studied did not drift or become more erratic over time. It can also be assumed that the independence assumption and constant variance assumption typical to this type of analysis are valid as the residual plots are structureless and contain no patterns for the most part.

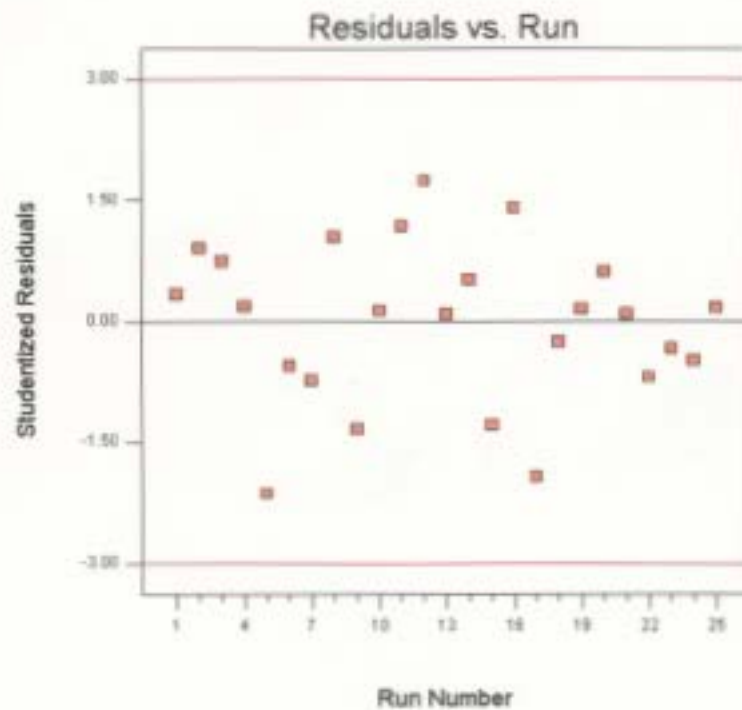


Figure B.3: Residuals vs. run

The predicted vs. actual graph shown in Figure B.4 shows that the model appears to predict quite well when the equation is used to predict the values shown at the different factor levels. The closer the data points follow a straight line, the better the model. The figure shows that the model seems quite accurate and is in good agreement with the previously mentioned  $R^2$  value.

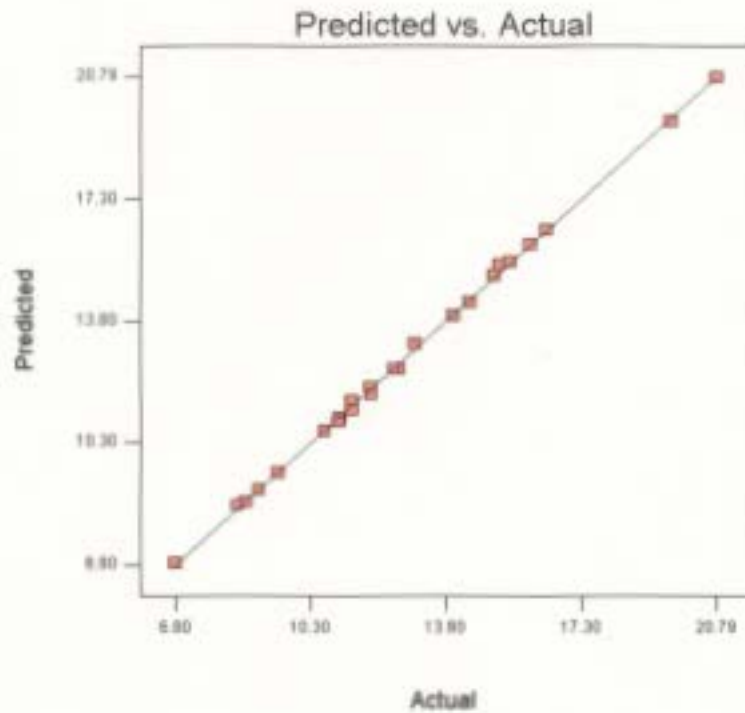


Figure B.4: Predicted vs. actual

Finally, a box-cox graph is utilized to determine if a transform is necessary. This is necessary when it appears that the model being developed is not linear. The box-cox graph attempts different powers, also known as alpha values, to try to fit a better curve. In this case, the box-cox graph has suggested an alpha value of 0.5. This is equivalent to stating that the root of the resonance frequency should be taken to make the model predict more accurately. This appears to make intuitive sense as resonance frequencies are definitely not linear as in equation B.1.

$$\omega_n = \sqrt{\frac{K}{M}} \quad (\text{B.1})$$

where

$\omega_n$  = resonance frequency [rad/s]

$K$  = spring constant [N/m]

$M$  = mass [kg]

To solve for the resonance, the square root of many dimensional factors contained within the spring constant,  $K$ , are taken in order to determine the resultant resonance frequency for a given mass,  $M$ . The equation determined by the DOE regression analysis is simply fixing scalar quantities to the dimensional variables that define  $K$ . The box-cox graph is shown below in Figure B.5. The transform (blue line) is regarded as satisfactory when it falls within the two confidence intervals (red lines).

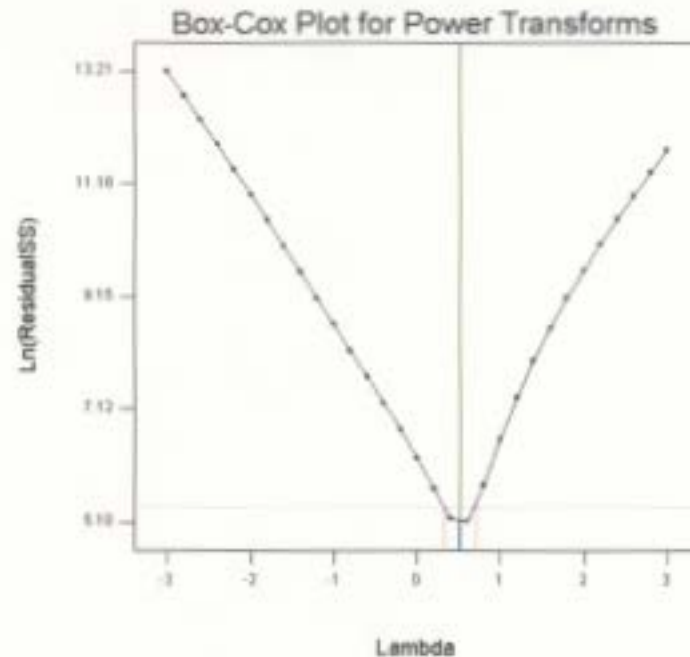


Figure B.5: Box-Cox graph

# Appendix C

## Bridge-Free AC-DC Power Conversion

Many researchers have tried to remove the bridge rectifier from the power harvesting circuitry with limited success. Unfortunately, these researchers have been tackling the problem by trying to remove the diode bridge electrically by using electronic switches and the like. Unfortunately, these switches require either boot energy or require far more energy than is actually produced by the energy harvester. However, the vertical motion of any vibrational energy harvester lends itself to the possibility of being a mechanical switch. Consequently, a method is proposed to eliminate the switch using MEMs technology. Figure C.1 (a) shows a proposed unimorph cantilever design. The only difference between this cantilever and previously discussed cantilevers is that there are two thin flexible wires attached to the cantilever: one on the top electrode of the cantilever, and one on the bottom electrode of the cantilever. The wiring scheme is shown in C.1 (b). This wiring scheme shows four separate electrodes, two on top and two on bottom, connected to a storage capacitor. The top left electrode connects to the positive terminal of the capacitor, while the top right electrode connects to the negative terminal. The bottom two electrodes are also wired to the capacitor, but are reversed.

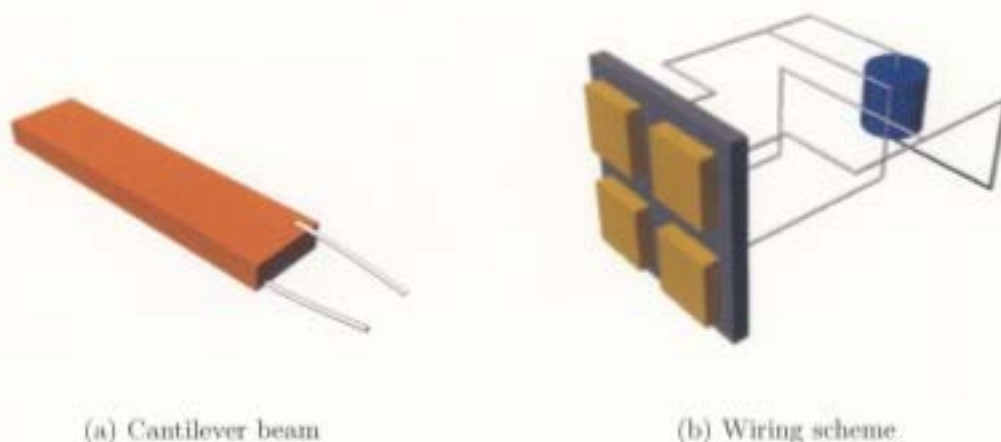
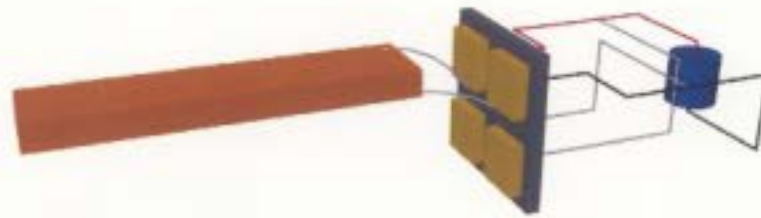


Figure C.1: Proposed mechanical-electrical design showing (a) thin conduction filaments on a cantilever beam and (b) electrical wiring

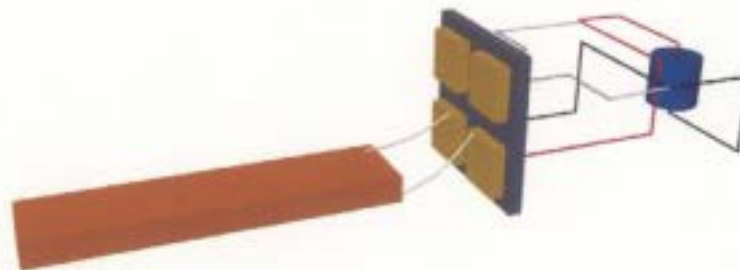
The process works as follows. First, the cantilever beam is positioned directly in the center of the four electrodes with neither of its flexible wires making any contact with either electrode. When the beam is excited and the end of the beam begins to move upward, the two flexible wires contact their respective top-right and top-left electrodes. This sends the first half cycle of the voltage produced by the piezo to the capacitor, which is positive in sign. This is shown in Figure C.2 (a). The path of current flow is shown by the colored sections of wire in the diagram. The red wire represents the hot wire, while the black represents the ground wire.

Next, the downward motion begins and the flexible wires hook into their two respective bottom electrodes as shown in Figure C.2 (b). Once again, the polarity of the voltage is shown by the colored sections of wire in the diagram. The only difference between the upward and downward cycle is that during the downward cycle, the voltage has a negative polarity. However, because these electrodes are wired in reverse order, the negative voltage appears as a positive voltage across the capacitor. Now, because the polarity is always positive across the capacitor, it can charge with close to no power losses. The only loss will be during the period when the beam is in its midpoint position and the wires are not touching either electrode. However,

this problem can be overcome by using MEMs technology to make the electrode gap and flexible wires as small as possible. In fact, with a very small electrode gap, the open circuit output of the energy harvester would look identical to the output of the bridge shown in Figure 4-10 (d).



(a) Upward position



(b) Downward position

Figure C.2: Proposed mechanical-electrical design showing (a) upward position and (b) downward position

Although the design shown in Figure C.1 is a unimorph beam, any number of layers can be used if wired correctly. Also, a cantilever design is shown for explanation purposes; however, a cymbal, carriage spring, inductive, capacitive, or magnetic energy harvester could all use a similar technique to mechanically eliminate the bridge. It should be noted that alternate designs could also be used, such as letting the flexible wires slide along the electrodes, or simply wiring all four electrodes appropriately and using a mercury switch. No matter what technique is used for a specific energy harvester, it is hypothesized that a vibration-excited energy harvester *can* be used as a mechanical switch to eliminate the bridge with little to no effect on the mechanical characteristics of the device. If this design could be implemented in practice, it is believed by the author that small amounts of *useful* power could be harvested from almost *any* vibration source, no matter how small. This concept of using mechanical switches instead of a bridge definitely warrants further investigation and would be an excellent area for future research.

# Bibliography

- [1] I. Buchman, “Is lithium-ion the ideal battery?” Sept. 2005. [Online]. Available: <http://www.adxs.com/pressreleases/2005-12-19.html>
- [2] S. J. Roundy, “Energy scavenging for wireless sensor nodes with a focus on vibration to electricity conversion, phd thesis,” Ph.D. dissertation, University of California, Berkeley, 2003.
- [3] “New version generates 3.6 times more power than predecessor, expanding alternative energy applications,” Dec. 19, 2005. [Online]. Available: <http://www.adxs.com/pressreleases/2005-12-19.html>
- [4] W. Sun, N. P. Kherani, K. Hirshman, L. L. Gadeken, and P. M. Fauchet, “A three-dimensional porous silicon p–n diode for betavoltaics and photovoltaics,” *Advanced Materials*, vol. 17, pp. 1230–1233, Feb. 2, 2005.
- [5] “Direct energy conversion technology,” 2004. [Online]. Available: <http://www.betabatt.com/>
- [6] A. Lal, H. Li, and H. Guo. “Integrated radioactive thin films for sensing systems.” in *Proceedings of the International Symposium on Circuits and Systems (ISCAS)*, May 23–26, 2004, pp. 596–599.
- [7] “Defense Advanced Research Projects Agency (DARPA),” 2006. [Online]. Available: <http://www.darpa.mil/>

- [8] W. Sun, N. P. Kherani, K. Hirshman, L. L. Gadeken, and P. M. Fauchet, "Analysis of a micro-electric generator for microsystems," in *The 8th International Conference on Solid-state Sensors and Actuators, and Eurosensors IX*, June 25–29, 1995, pp. 369–372.
- [9] R. Amirtharajah and A. P. Chandrakasan, "Self-powered signal processing using vibration-based power generation," *IEEE Journal of Solid-State Electronics*, vol. 33, no. 5, pp. 687–695, May 1998.
- [10] T. Eggborn, "Analytical models to predict power harvesting with piezoelectric materials, msc. thesis," Master's thesis, Virginia Polytechnic Institute and State University, May 2003.
- [11] "Piezoelectricity," 2005. [Online]. Available: <http://www.americanpiezo.com>
- [12] H. S. Tzou, *Piezoelectric Shells: Distributed Sensing and Control of Continua*. Massachusetts : KluwerAcademic, 1993.
- [13] M. Umeda, K. Nakamura, and S. Ueha, "Analysis of transformation of mechanical impact energy to electrical energy using a piezoelectric vibrator," *Japan Journal of Applied Physics*, vol. 35, no. 5B, pp. 3267–3273, 1996.
- [14] M. Umeda, S. Ueha, and K. Nakamura, "Energy storage characteristics of a piezo-generator using impact vibration," *Japan Journal of Applied Physics*, vol. 36, no. 5B, pp. 3146–3151, May 1997.
- [15] J. Kymissis, C. Kendall, J. Paradiso, and N. Gershenfeld, "Parasitic power harvesting in shoes," in *Second International Symposium on Wearable Computers*, Oct. 19–20, 1998, pp. 132–139.
- [16] A. Kasyap, J. Lim, K. Ngo, A. Kurdila, T. Nishida, M. Sheplak, and L. Cattafesta, "Energy reclamation from a vibrating piezoceramic composite beam," in *9th International Congress on Sound and Vibration*, July 2002.

- [17] G. K. Ottman, H. F. Hofmann, A. C. Bhatt, and G. A. Lesicutre, "Adaptive piezoelectric energy harvesting circuit for wireless remote power supply," *IEEE Transactions on Power Electronics*, vol. 17, no. 5, pp. 669–676, Sept. 2002.
- [18] "The Mathworks Inc." 2006. [Online]. Available: <http://www.mathworks.com/>
- [19] "Solutions for control," 2006. [Online]. Available: <http://www.dspaceinc.com>
- [20] G. K. Ottman, H. F. Hofmann, and G. A. Lesicutre, "Optimized piezoelectric energy harvesting circuit using step-down converter in discontinuous conduction mode," *IEEE Transactions on Power Electronics*, vol. 18, no. 2, pp. 696–703, Mar. 2003.
- [21] "Wolfram Inc." 2006. [Online]. Available: <http://www.wolfram.com/>
- [22] S. Roundy, P. K. Wright, and J. Rabaey, "A study of low level vibrations as a power source for wireless sensor nodes," *Computer Communications*, vol. 26, pp. 1131–1144, Oct. 2003.
- [23] S. Roundy and P. K. Wright, "A piezoelectric vibration based generator for wireless electronics," *Smart Materials and Structures*, vol. 13, pp. 1131–1142, Aug. 2004.
- [24] A. Dogan, K. Uchino, and R. E. Newnham, "Composite piezoelectric transducer with truncated conical endcaps "cymbal"," *IEEE Transactions on ultrasonics, ferroelectrics, and frequency control*, vol. 44, no. 3, pp. 597–605, May 1997.
- [25] J. F. Tressler, W. Cao, K. Uchino, and R. E. Newnham, "Finite element analysis of the cymbal-type flextensional transducer," *IEEE Transactions on ultrasonics, ferroelectrics, and frequency control*, vol. 45, no. 5, pp. 1363–1369, Sept. 1998.
- [26] H. W. Kim, A. Batra, S. Priya, K. Uchino, D. Markley, R. E. Newnham, and H. F. Hofmann, "Energy harvesting using a piezoelectric "cymbal" transducer

- in dynamic environment,” *Japanese Journal of Applied Physics*, vol. 43, no. 9A, pp. 6178–6183, Sept. 1998.
- [27] K. Deng and C. Shippis, “Wireless sensing nodes powered by piezoelectric vibration energy harvesting devices,” in *59th Meeting of the Society for MFPT*, Apr. 18–21, 2005, pp. 593–602.
- [28] “Ansys verification manual.” pp. 1.1–1.2, 2006. [Online]. Available: [http://www.oulu.fi/tietohallinto/ohjeet/unix/ansys-6.1/content/Hlpunderscore\\_V\\_VMTOC.html](http://www.oulu.fi/tietohallinto/ohjeet/unix/ansys-6.1/content/Hlpunderscore_V_VMTOC.html)
- [29] V. Schmidt, “Theoretical electrical power output per unit volume of pvt and mechanical-to-electrical conversion efficiency as functions of frequency,” in *Proceedings of the Sixth IEEE International Symposium on Applications of Ferroelectrics*, 1986, pp. 538–542.
- [30] “Piezo Systems Inc. Catalog No. 6,” pp. 23–25, 2005. [Online]. Available: <http://www.piezo.com/Catalog6b.pdf>
- [31] “TRS advanced materials overview,” 2006. [Online]. Available: <http://www.trsceramics.com/materials.php>
- [32] S. Imaoka, “Collaborative Solutions Inc. Ansys tip of the week: Conversion of piezoelectric material data,” Nov.12 1999. [Online]. Available: [http://ansys.net/ansys/tips/Week13\\_TNT\\_Conversion\\_of\\_Piezoelectric\\_Material\\_Data.pdf](http://ansys.net/ansys/tips/Week13_TNT_Conversion_of_Piezoelectric_Material_Data.pdf)
- [33] “Ansys element reference.” p. 2.5.6, 2006. [Online]. Available: [http://www.oulu.fi/tietohallinto/ohjeet/unix/ansys-6.1/content/Hlpunderscore\\_E\\_ElemTOC.html](http://www.oulu.fi/tietohallinto/ohjeet/unix/ansys-6.1/content/Hlpunderscore_E_ElemTOC.html)
- [34] D. C. Montgomery, *Design and Analysis of Experiments*. John Wiley and Sons Inc., 2001.

- [35] “Stat-Ease Inc.” 2006. [Online]. Available: <http://www.statease.com/>
- [36] D. J. Ewins, *Modal Testing: Theory and Practice*. Research Studies Press Ltd., 1995.
- [37] J. Siebert, J. Collier, and R. Amirtharajah, “Self-timed circuits for energy harvesting ac power supplies,” in *ISLPED 2005*, Aug. 8–10, 2005, pp. 315–318.







